Improving High-Latitude Sea Surface Height Data Assimilation: Part II Model Based Vertical Covariance

Robert W. Helber,[a] Elizabeth M. Douglass,[a] Xiaobiao Xu,[b] Julie L. McClean,[c] Eric P. Chassignet,[b] Alan J. Wallcraft,[b], and Alexandra Bozec[b]

[a] *Naval Research Laboratory, Stennis Space Center, MS*

[b] *Center for Ocean-Atmospheric Prediction Studies, Florida State University, Tallahassee, FL*

[c] *University of California San Diego, Scripps Institution of Oceanography, La Jolla, CA*

Corresponding author: Robert W. Helber, robert.w.helber.civ@us.navy.mil

ABSTRACT

The most important source of information constraining the Navy's operational global ocean forecasting system is sea surface height anomaly as measured by satellite altimetry. These observations inform a one-dimensional variational analysis to create synthetic profiles of temperature and salinity that are assimilated as observations in a three-dimensional variational assimilation analysis. The 1D analysis requires vertical error covariances that relate the differences in values between temperature and salinity at different depths. These vertical covariances are computed empirically from historical in situ observation profiles of temperature and salinity. The approach ensures that the synthetics have realistic structure without drifting. A shortcoming of this approach is the availability of in situ observations extending at least 1000 m deep. Observations are sparser at high latitudes, often do not include salinity, and reach relatively shallow depths. We wish to use model data to address these limitations. Here we show that using a global 30-year model run to compute vertical covariances solves sampling issues while continuing to maintain accuracy. While the covariances derived from the model generally compare well with the observed ones, in some areas of the ocean, the numerical ocean model has different vertical covariances. A new method for determining where synthetics are most valuable is presented. The implication of having model derived covariances is the ability to extend covariance information at high latitude where in situ observations are sparce or have sampling anomalies. Results also suggest that salinity, if observed, would provide substantial improvement to the system.

SIGNIFICANCE STATEMENT

The purpose of this study is to understand present high northern latitude ocean numerical forecasting capabilities and shortcomings related to the use of sea surface height measurements derived from satellite, which are used to correct ocean forecast models that diverge from reality due to chaos. This is important because changing conditions are amplified at high latitudes and require modifications to present forecasting systems. Ocean forecasting is challenging in these regions due to few in situ observations and unique oceanographic conditions. Our paper describes new methods in data poor regions and more accurate model uncertainty estimates for maximizing forecast capabilities.

1. Introduction

The most important source of observational information used to constrain mesoscale variability in operational, data assimilative, ocean forecasting systems is sea surface height anomaly (SSHA) as measured by satellite altimetry. SSHA data is typically assimilated using empirically derived covariances (Miyazawa et al. 2009) and ensemble optimal interpolation methods (Oke et al. 2008) that modify the interior physical variables (temperature, salinity, velocities) so that their temperature and salinity profile anomaly gives rise to a steric SSHA that matches the observed SSHA. The method used by the US Navy differs in the sense that the operational implementation of SSHA data assimilation employs a one-dimensional (1D) variational approach to create synthetic ocean profiles of temperature and salinity (Helber et al. 2013) that are then assimilated as observations in a three-dimensional variational (3DVAR) assimilation system (Metzger et al. 2014). The advantage of this approach for assimilated SSHA data are the constraints to the climatological mean and vertical structure. The synthetics are created as anomalies from climatology and thus maintain realistic structure that will not drift. While this system for assimilation of SSHA data into ocean models works well for most of the ocean (Thoppil et al. 2021), it may not be optimal for the Arctic and sub-Arctic Seas because the climatological information is less reliable due to poor data sampling and rapidly changing conditions. To understand how these limitations impact the success of the assimilation scheme, this paper, the second in a two-paper series, describes research for improving high-latitude SSHA data assimilation in ocean forecasting of the Arctic and sub-Arctic Seas, northward of 40ºN. The Part 1 paper describes selective usage of synthetic ocean profiles analyzed within an Observing System Simulation Experiment (OSSE) framework (Douglass et al. 2025; hereafter Part 1) while the present manuscript focuses on the synthetic generation system itself. The end goal of this research is to create accurate, data assimilative ocean forecasts for the Arctic and sub-Arctic Seas.

At the core of the Navy's SSHA data assimilation approach is empirical vertical covariance information derived from historical in situ observational temperature and salinity profiles from the Navy's Master Oceanographic Observation Data Set (MOODS)(Bauer 1985; Teague 1987). The covariances are essential in the 1D variational methods for creating the synthetics. The observed in situ profiles, composed of conductivity, temperature, and depth (CTD), expendable bathythermographs (XBT), mooring, and glider profiles, and other data from profiling observation systems, provide relatively high-vertical resolution profiles at a coarse non-uniform, horizontal and temporal sampling coverage. Figure 1 shows the number of profiles, in ½ degree bins, used in the Navy's Improved Synthetic Ocean Profile system version 1 (ISOP1) (Helber et al. 2013). Many of the observations occur where research vessels have sailed, but many of the observations occur randomly as sampled by the Argo autonomous vertical-profiling float program. There are many more profiles near the coasts in the northern hemisphere. Also, the sampling is non-uniform and in the vertical, the number of observations decreases with depth. The end result is a dataset that resolves the mesoscale vertical structure over most of the ocean that we use to create vertical correlation estimates in monthly climatological averages. However, at high latitude, these observations have a pattern that decreases in number toward the north pole, making it hard to resolve the mesoscale vertical structure in the Arctic and sub-Arctic Seas. Furthermore, sea surface height data assimilation at high latitude is severely limited by the available satellite sea surface height anomaly (SSHA) observations which are unavailable northward of approximately 75ºN. In addition, the Navy operational system currently turns off synthetic profiles derived from SSHA if the vertical ocean stratification is small [see Part 1 for a detailed discussion] (Figure 2). This was implemented because of the perception that these profiles were unreliable under this condition. In Figure 2, the grey areas have ice coverage for January 3rd, 2017 and thus areas where synthetics are not created are ice free. A key goal of this research is to extend SSHA data assimilation into the areas that are presently neglected, as shown in Figure 2a.

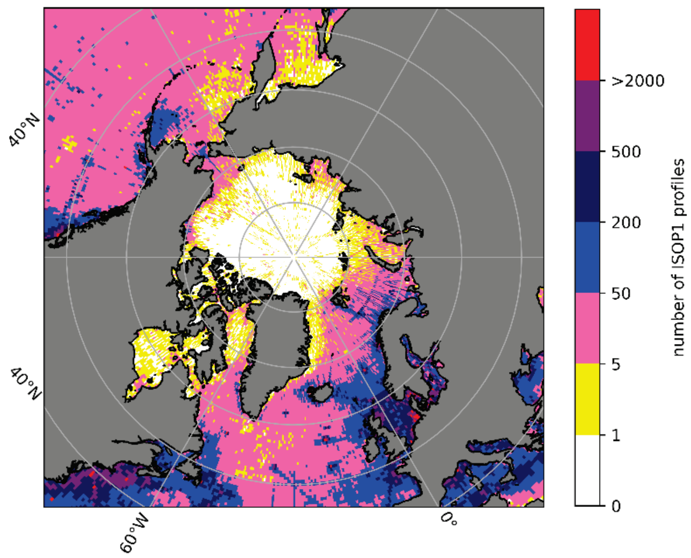

Fig. 1. The number of in situ observations in 1/2º squares in the ocean. The data numbers shown are from the database used to create ISOP1.

The current Navy approach relies on historical observations, but given the latest advancement in ocean modeling, one can envision that the mesoscale vertical error covariances could be derived from multi-decadal high-resolution global ocean models (Chassignet et al. 2020) as long as the models have been shown to be representative of the observed variability. In this paper, we explore the option of replacing the in situ observations, in the calculation of the ISOP vertical error covariances, with global ocean modeling high-resolution 1/12º data created using the Hybrid Coordinate Ocean Model (HYCOM) (Bleck 2002; Chassignet et al. 2003) over the 1958-2022 time period (Chassignet et al. 2020). The advantage of this approach is that the model has uniform coverage of the global ocean in space and time, including at high latitude where in situ observations are sparse. Thus, at high latitude, we will have significantly more model output than in situ observations. A potential drawback, however, is that the model results may not accurately represent all the variability that occurs in the ocean, due to its limited horizontal resolution, approximate parameterizations, missing physics, inaccurate bathymetry and forcing, etc.

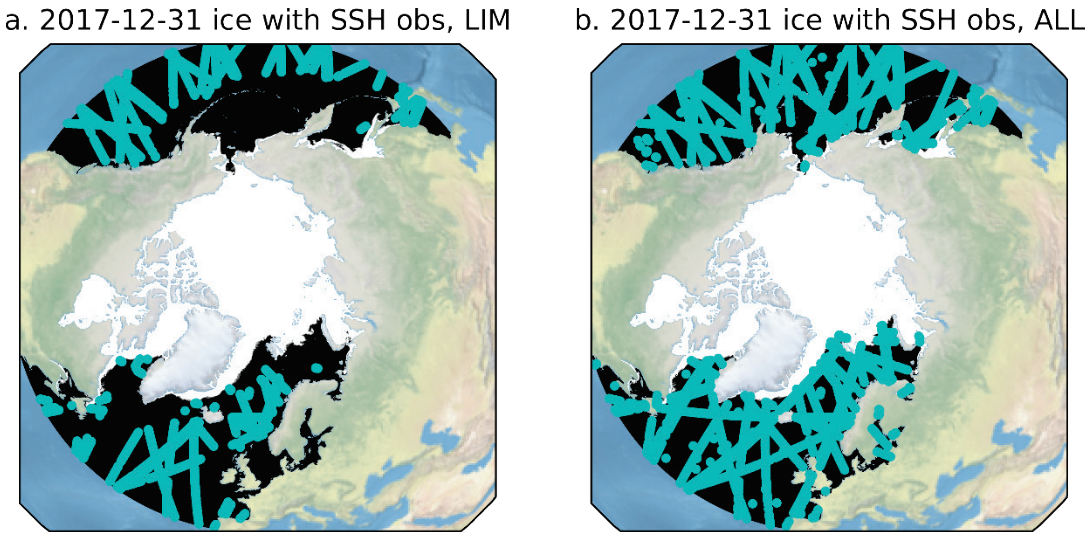

Fig. 2. The locations of synthetic profiles (cyan dots) and the ice coverage (white ocean areas) on January 3rd, 2017. On the left (a), the synthetic profiles are restricted because of low stratification. On the right (b), the synthetic profiles are not restricted and are produced further northward.

In Section 2, we describe the methods used for creating ISOP1 synthetic ocean profiles from inputs of SSHA, sea surface temperature, and mixed layer depth. The methods for computing vertical covariances, the correlation length scales, extracting model data for five sampling fidelity test cases, and validating the results relative to observational profiles are also discussed in section 2. Section 3 describes the validation, relative to independent in situ observations, of the new model formulated synthetics compared to traditional observation-based methods. Also in Section 3, we describe the Observing System Simulation Experiment (OSSE) for the Arctic and sub-Arctic Seas described in Part 1 (See also Fine et al. 2023) that utilizes the new model-based synthetics. We discuss the practical application of this system at high latitudes and in regions of the ocean where the HYCOM model data may provide the greatest advantages over insufficient in-situ observations. Finally, we explore veracity of the synthetics relative to the temperature and salinity properties over the water column and suggest a new method for determining when synthetics are most accurate. Section 4 contains a summary and conclusions for this research.

2. Methods

2.1 Synthetics Profile Methods

The system for constructing synthetic profiles from surface observations uses real time inputs of sea surface temperature (SST), $\tilde{T}_1$ and height anomaly, $\delta\tilde{h}$, and an estimate of the surface mixed layer depth (MLD). The cost function, to create one synthetic profile at a location, is given by

$$
\begin{aligned}
J = {} & \delta\mathbf{x}^{(clim)T}\mathbf{B}^{-1}\delta\mathbf{x}^{(clim)} + \delta\mathbf{d}^{(\mathrm{clim})T}\mathbf{B}^{(\mathbf{d})-1}\delta\mathbf{d}^{(\mathrm{clim})} \\
& + \delta\mathbf{x}^{(eof)T}\mathbf{V}^{-1}\delta\mathbf{x}^{(eof)} + \delta\mathbf{d}^{(eof)T}\mathbf{V}^{(\mathbf{d})-1}\delta\mathbf{d}^{(eof)} \\
& + \delta\tilde{T}_1^{(obs)}R^{(SST)-1}\delta\tilde{T}_1^{(obs)} + \left(\mathbf{L}\delta\mathbf{x}^{(clim)} - \delta\tilde{h}^{(\mathrm{clim})}\right)R^{(SSHA)-1}\left(\mathbf{L}\delta\mathbf{x}^{(clim)} - \delta\tilde{h}^{(\mathrm{clim})}\right).
\end{aligned} \tag{1}
$$

The first two terms on the right-hand-side of equation 1 contain the deviation of the solution from climatology, $\delta\mathbf{x}^{(\mathrm{clim})}$, and the deviation of the vertical difference of the solution from that of climatology, $\delta\mathbf{d}^{(clim)}$. The background error covariance and the background vertical difference error covariance are $\mathbf{B}^{-1}$ and $\mathbf{B}^{(d)-1}$, respectively. The next two terms are the deviation of the reduced empirical orthogonal function (EOF) mode, solution from climatology, $\delta\mathbf{x}^{(eof)}$, and the deviation of the reduced empirical orthogonal function (EOF) mode, vertical difference of the solution from that of climatology, $\delta \mathbf{d}^{(eof)}$. The diagonal matrix of variances and the vertical difference diagonal matrix of variances are $\mathbf{V}^{-1}$ and $\mathbf{V}^{(d)-1}$, respectively. The first two terms on the right-hand-side of equation 1 contain the deviation of observed SST from the solution, $\delta \tilde{T}_1^{(obs)}$, the deviation of observed SSHA from the climatology, $\delta \tilde{h}^{(\mathrm{clim})}$, and the deviation of climatological SSHA from the solution, $\mathbf{L}\delta \mathbf{x}^{(\mathrm{clim})}$. The diagonal matrix of SST error variance and the diagonal matrix of SSHA error variance are $R^{(SST)}$ and $R^{(SSHA)}$, respectively. Equation 1 and these variables are described in more detail in the Appendix.

A key component of this one-dimensional variation analysis is the vertical covariance model derived from empirical in situ observations, which resolve the mesoscale vertical structure over most of the ocean. The vertical covariances enable the minimization of equation 1 to project the surface information downward into the ocean to create a synthetic profile that is statistically consistent with the mesoscale vertical structure. In some regions of the ocean, such as the Arctic and sub-Arctic seas, in situ observations are not plentiful enough to provide adequate vertical covariances. Thus, in this research we investigate the feasibility of using global model data to create vertical covariance data.

The vertical covariances are split into correlations and variances such that

$$\mathbf{B} = \mathbf{UCU}, \tag{2}$$

where the monthly climatological standard deviation is $\mathbf{U}$ and monthly climatological correlation is $\mathbf{C}$.

A key component of making synthetics is the structure of the vertical covariances $\mathbf{B}$ and $\mathbf{B}^{(\mathbf{d})}$. Each of those have both variances and correlations. An example of correlations from a high latitude location (3ºE, 70ºN) is shown in Figure 3 and the climatological standard deviation is shown in Figure 4. The data used to construct these covariances are from the original ISOP1 data shown in Figure 1. At this location, the correlations were computed from 294 in situ profiles observations within a 2º search radius. The data for the correlation is weighted by the distance from the analysis location.

The auto-correlations in Figure 3 c and b, have diagonal elements that are nearly one, but not exactly one, because the correlations are constructed from six EOF modes, for reduction in data storage. The cross-correlations for S with T (Figure 3d) and T with S (Figure 3a) are transposes of each other. The depth of the climatological mixed layer for June can be seen most clearly in the salinity auto-correlation (Figure 3b), where the mixed layer is negatively correlated with the deep ocean, in the Lofoten Basin at 3ºN, 70ºW (Raj et al. 2020). The vertical difference correlations (see the Appendix; Figure A1) have substantially different structure that represents persistent gradients and inflection points, on average, found in the historical profiles.

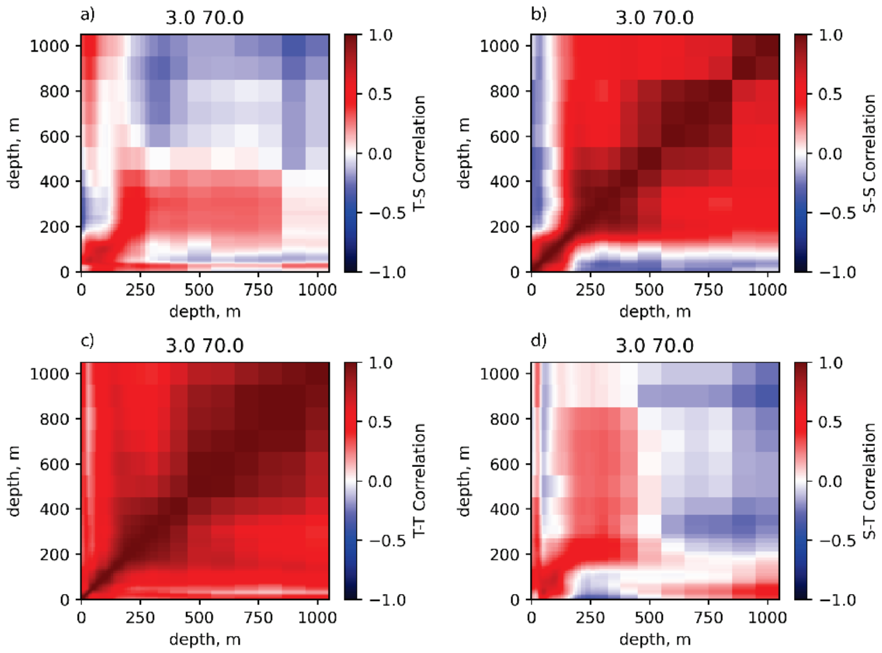

Fig. 3. The vertical correlations for T and S at 3ºE, 70ºN for June. The auto-correlations for T and S are along the diagonal in panels b and c. The off-diagonal cross-correlations for S with T and T with S are in panels a and d. Since the correlations go from 0 to 1000 m, the x and y axes cover the same depths. The block structure indicates there are 47 depth levels in the upper 1000 m, where the block indicates depth bins that get larger increasing with depth. At this location, the correlations were computed from 294 in situ profile observations.

As shown in equation 2, the covariance is the correlation multiplied by the diagonal variance, $\mathbf{U}$, which contains both the T and S variances along the diagonal (see the Appendix). The square root of the variance (standard deviation), for T and S, at the location 3ºE, 70ºN, in the Lofoten Basin of the Norwegian Sea, is shown in Figure 4. One characteristic of this location in the ocean is that the largest standard deviation occurs at the surface, as compared to the mid-latitude ocean where the largest variance occurs in the thermocline (Helber et al. 2023).

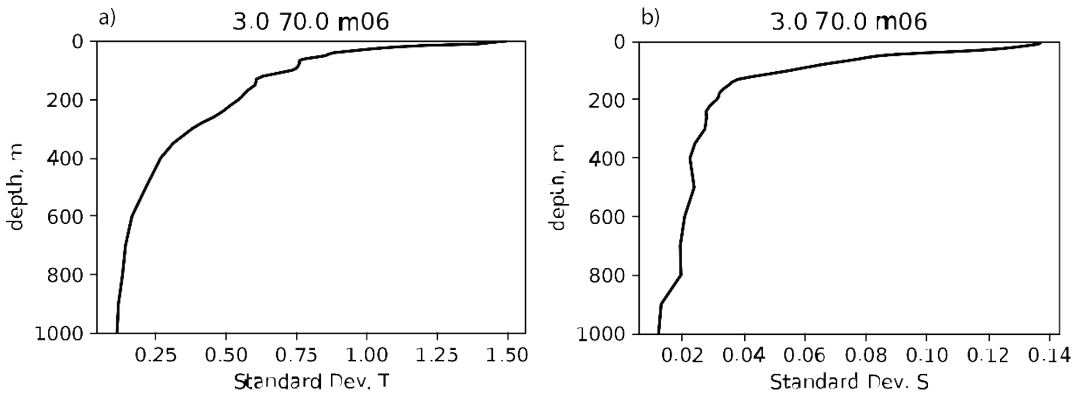

Fig. 4. The standard deviation profile for T and S for June at 3ºE, 70ºN, corresponding with the correlations shown in Figure 3.

The covariances are constructed from MOODS data for each month at every ½ degree location in the ocean. To help visualize the spatial variability of the correlations, we integrate the correlation at depth k with all the other depths, thereby providing a single number to represent the nature of the correlation at each grid point. For each of the correlation components in equation (2) we compute

$$\bar{C}_k = \frac{\sum_{i=2}^{nz} C_{ik}\left|z_i - z_k\right|}{\sum_{i=2}^{nz}\left|z_i - z_k\right|} \tag{3}$$

where C_{ik} is the correlation between depth i and depth k. Thus $\bar{C}_k$ is the depth average correlation relative to depth level k. To obtain a characteristic correlation over the full water column down to 1000 m we compute a depth-weighted average correlation such that

$$\bar{C} = \frac{\sum_{i=2}^{nz} \bar{C}_k \Delta z_i}{\sum_{i=2}^{nz} \Delta z_i}, \tag{4}$$

where $\Delta z_i = z_i - z_{i+1}$ is the distance between each depth grid level. If every depth level were perfectly correlated with each other depth, the correlation would be 1.

To show the spatial variability of the average T versus S cross-correlation, we plot the vertically averaged correlation (equation 4) at each grid point for the months of February, May, August, and November (Figure 5). Notice that there is modest seasonality in the vertically averaged correlation, computed from the ISOP1 dataset. During the rest of the year, there is not enough data in the Arctic to compute vertical correlations. The blue areas indicate that much of the T versus S cross-correlations with depth are negative, such as in the Gulf of Alaska. In the next section we will describe additional sets of data sources and sampling strategies that allows us to demonstrate the effectiveness of model based covariances and the role of shifting climate.

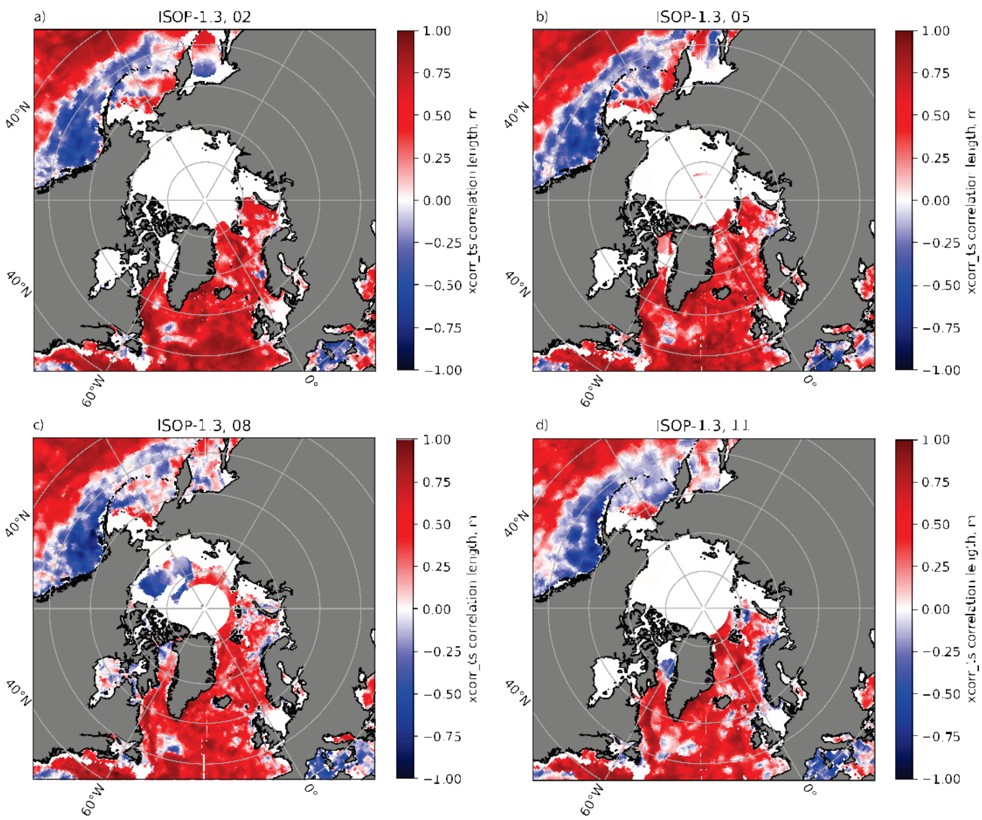

Fig. 5. Depth average cross-correlation for T and S at each grid point for the months of a) February, b) May, c) August, and d) November.

2.2 Data Sampling Strategies

For ISOP1, the fidelity of the MOODS observations was determined by the available data collected at random locations around the global ocean up until the calendar year 2008. Using HYCOM model data, however, we are not restricted to the location of the in situ observations. The model output for the full grid domain cover years from 1964 through 2022. To evaluate the impact of spatial sampling, we extract the model data in three different levels of fidelity. The “obs-obs” fidelity is to extract the model data at the ISOP1 observation locations, at the observation depths. Since the model has full water column coverage over the global ocean, we also extract full water depth model data at the observation locations (called “obs-full”). The horizontal distribution of these data are the same as that for ISOP1 in Figure 1. Then, to take advantage of the higher fidelity of the model data, we extract model data at ½ degree resolution, globally every 10 days for 36 samples a year (called “05deg”). The result of this selection was too much data for our analysis programs. For this reason, we randomly in time subsampled these data keeping 10% of the total number of profiles. This approach results in a data set with roughly 200 profiles per ½ degree bin. Thus, this 10% randomly subsampled data set has a uniform distribution of profiles globally (Figure 6). Near the coast, however, there are more profiles in the in situ observed data set, as can be seen the yellow areas of difference between the “05deg” minus the ISOP1 “obs” sampling in Figure 6b. The sampling strategy for the model-based covariances HYCOM-obs-obs and HYCOM-obs-full used data for the period from 1964 through 2008, to match, the ISOP1 in situ observation period. The case HYCOM-05deg data period was from 1964 to 2016. To evaluate longer term shifts in the ocean’s covariance state, we include a test case HYCOM-last-decade, which used data from 2013 through 2022. Because of the shorter time length, we increased the percentage to 20% of the initial 10-day sampling rate. There is a new version of ISOP2 that has newer observations with the distribution shown in Figure 7. Overall, there is an increase in the number of profiles, with a modest increase in the Arctic. The list of data fidelity and sampling strategy is shown in Table 1.

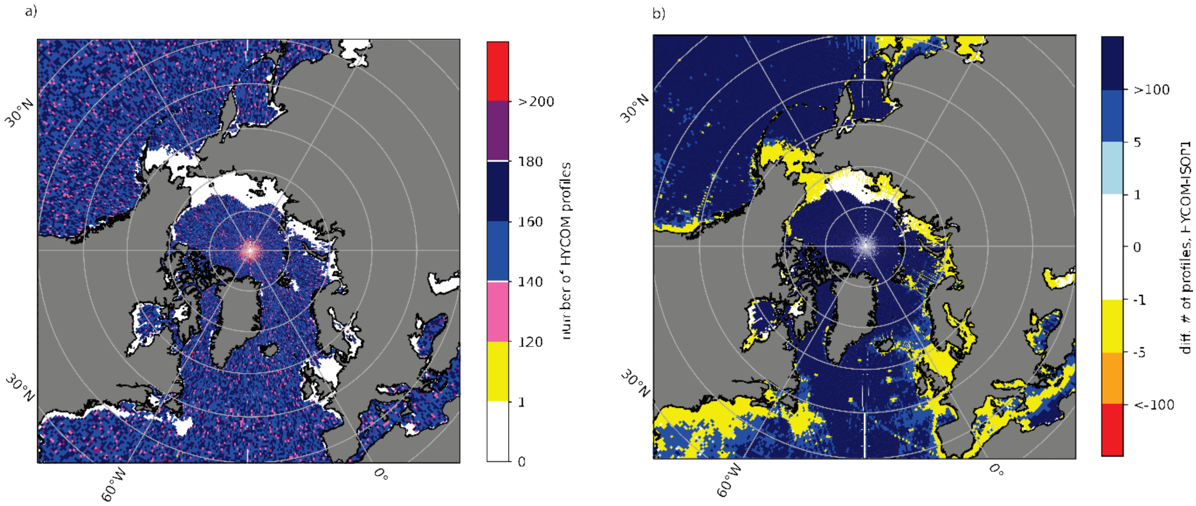

Fig. 6. The number of in situ observations in 1/2º squares in the ocean. The data numbers shown in a) are from the HYCOM data for 10% of the 0.5 selection (see text and Table 1). The numbers shown in b) are for the difference in the number of profiles for HYCOM-05deg minus ISOP1.

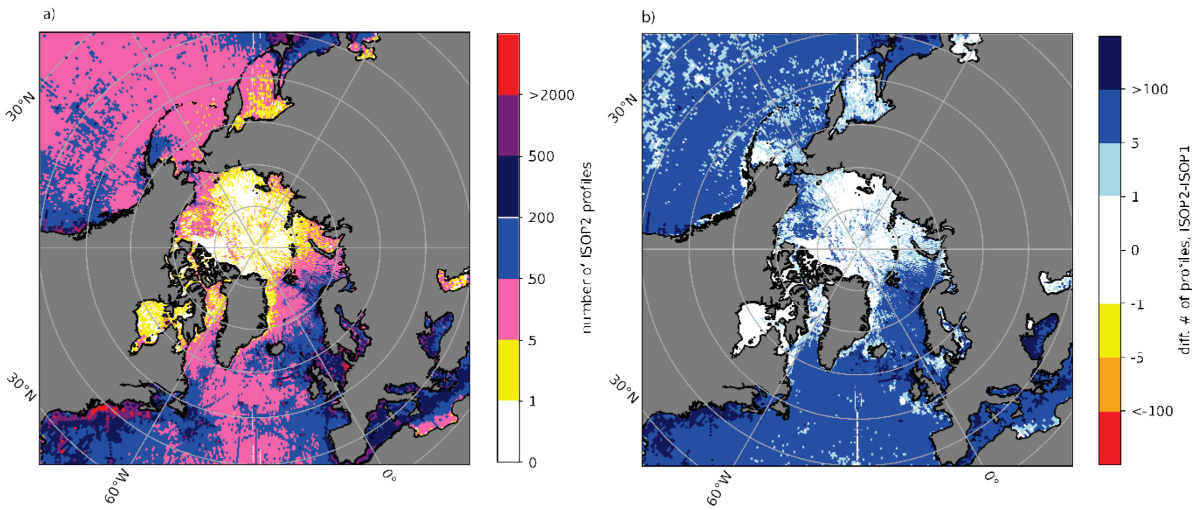

Fig. 7. The number of in situ observations in 1/2º squares in the ocean. The data numbers shown in a) are from the database used to create the Improved Synthetic Ocean Profiles (ISOP) system version 2. The numbers shown in b) are for the difference in the number of profiles for ISOP2 minus ISOP1.

Label	**Source**	**Date Range**	**Depths**	**Fidelity Location**
ISOP1	OBS	<1920-2008	OBS	OBS (ISOP 1)
ISOP2	OBS	<1920-2019	OBS	OBS (ISOP 2.1)

HYCOM-obs-obs	HYCOM	1964-2008	OBS	OBS (ISOP 1)
HYCOM-obs-full	HYCOM	1964-2008	MODEL	OBS (ISOP 1)
HYCOM-05deg	HYCOM	1964-2016	MODEL	10% of 0.5º selection
HYCOM-last-decade	HYCOM	2013-2022	MODEL	20% of 0.5º selection

Table 1. List of covariance data set features.

To see the effect of the sampling strategy on the correlation length scales, we plot the cross-correlation length (equation 4) for the ISOP1, ISOP2, HYCOM-obs-obs, and HYCOM-05deg test cases in Figure 8. We see that the ISOP1 sampling strategy has the fewest valid correlation values in the Arctic ocean. To make valid T/S cross-correlations, observations must have good values over the entire depth range to 1000 m. In the Arctic, HYCOM is more reliable in this way. The original ISOP1 data was limited in the Arctic (Figure 8a). The ISOP2 sampling strategy has good coverage in the Arctic and the HYCOM-05deg case has the greatest coverage. In the central Arctic, HYCOM-05deg shows a positive T/S cross-correlation, whereas the ISOP2 data have a negative cross-correlation. This also occurs in Baffin Bay, where the HYCOM-obs-obs and the HYCOM-05deg, both have negative cross correlations whereas ISOP1 has positive. In these regions, the HYCOM derived solution has the opposite sign compared to the observed data.

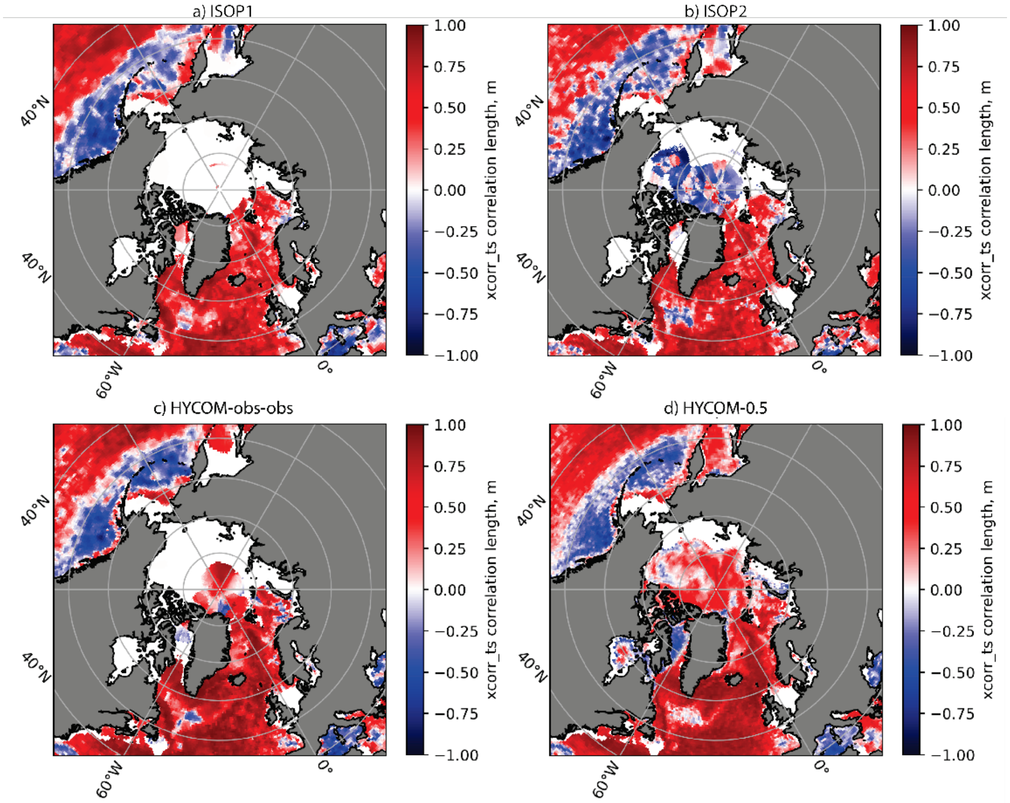

Fig. 8. The temperature vs salinity cross-correlation for (a) ISOP1, (b) ISOP2, (c) HYCOM-obs-obs, and (d) HYCOM-05deg at each ½ degree grid point for the Arctic Ocean and the sub-polar seas for May.

3. Synthetic Profile Validation

2.1 Test Cases

To evaluate the quality of synthetic profile generation for each case, we use a method for creating synthetics to match actual observed in situ profiles. To do this we create synthetic profiles using inputs from MOODS observed in situ profiles, that are not included in creation of the covariances. The MOODS profiles we use, for the years 2019, 2020, and 2020 are independent from the data used to create the covariances. The inputs for SST, MLD and SSHA used to create the synthetics come from the MOODS T and S profiles for each case listed in Table 1. SST is taken from the shallowest T in the profile and the MLD and SSHA are computed from the observed profile. All profiles selected for this purpose have both T and S, have a value at least 12 m from the surface, and extend to at least 1000 m. Thus, for each observed profile, we have a matching synthetic for each case. These synthetics represent the best possible representation of the profiles that the system can create, since the inputs come directly from the profiles themselves. The annual mean steric height (see the Appendix) comes from the Navy's Generalized Digital Environmental Model (GDEM) ocean climatology, version 4 (GDEM4) (Carnes et al. 2010). The synthetic validation cases are listed in Table 2.

Case name	SST source	STHT Monthly	STHT annual	STHT	SSHA	Vert. Covariance
	$T_1^{(obs)}$	$h^{(\mathrm{clim})}$	$h^{(annual4)}$	$\tilde{h}$	$\delta\tilde{h}$	$\mathbf{B} = \mathbf{UCU}$
ISOP1	OBS SST	ISOP1 data	GDEM4 annual STHT	OBS T/S profile	$\tilde{h} - h^{(annual4)}$	ISOP1 dat
ISOP2	OBS SST	ISOP2 data	GDEM4 annual STHT	OBS T/S profile	$\tilde{h} - h^{(annual4)}$	ISOP2 data
HYCOM-OBS-OBS	OBS SST	HYCOM-OBS-OBS data	GDEM4 annual STHT	OBS T/S profile	$\tilde{h} - h^{(annual4)}$	HYCOM-OBS-OBS data
HYCOM-OBS-FULL	OBS SST	HYCOM-OBS-FULL data	GDEM4 annual STHT	OBS T/S profile	$\tilde{h} - h^{(annual4)}$	HYCOM-OBS-FULL data
HYCOM 05deg	OBS SST	HYCOM 05deg data	GDEM4 annual STHT	OBS T/S profile	$\tilde{h} - h^{(annual4)}$	HYCOM 05deg data
HYCOM 05deg L-DEC	OBS SST	HYCOM 05deg Last Decade data	GDEM4 annual STHT	OBS T/S profile	$\tilde{h} - h^{(annual4)}$	HYCOM 05deg Last Decade data

Table 2. Synthetic versus MOODS validation cases including the source of steric height (STHT), monthly and annual average and the background vertical covariances.

The only difference between each of the test cases described in Table 2, is the vertical error covariance data used to make the synthetics and the internal reference monthly steric height (STHT Monthly; $h^{(\mathrm{clim})}$) as described above and in the Appendix. Part of the calculation of the monthly vertical error covariance is the monthly mean and variance of the data used to create the correlations. As explained in the appendix, there is also a term in equation A16 that involves the monthly mean steric height, $h^{(\mathrm{clim})}$, which is computed from the same data used to make the covariances. The annual mean steric height, however, is computed from the GDEM version 4 ocean climatology of T and S. Thus, there is a difference in the origin of the climatological mean versus the annual mean steric height for all cases except for the ISOP1 test case. In the case of ISOP1, the annual and monthly climatological mean steric height is computed from the same data. In all other cases, these two quantities are slightly different. This difference is minor since the monthly climatological mean anomaly is separate from the annual mean anomaly. The system equates the consistent anomalies, not the total steric height. The synthetic steric height anomaly is equated with the satellite SSH anomaly. While this inconsistency is likely negligible, this fact could put the HYCOM test cases at a slight disadvantage. The difference between a model versus in situ derived steric height could be larger, giving the HYCOM test cases slightly larger errors.

To summarize the errors, we compute the σ_0 (surface referenced potential density) Root Mean Square Error (RMSE) over depth for each profile, binned in 1-degree boxes northward of 40ºN (Figure 9). The number of observations in each box is shown in Figure 9a. The test cases where the covariances are derived from in situ observations, ISOP1 and ISOP2 test cases (Figure 9, b and c), there are more light blue boxes in the Gulf of Alaska and Bering Sea. This indicates ISOP1 and ISOP2 have smaller RMSE values compared to the HYCOM data cases, in these areas. The RMSE values are comparable in the Atlantic Ocean, Irminger Basin, and the Greenland Sea, in all test cases. Unfortunately, there are few validation profiles in the Arctic Ocean and the Baffin Bay. Thus, these two regions cannot be evaluated for veracity.

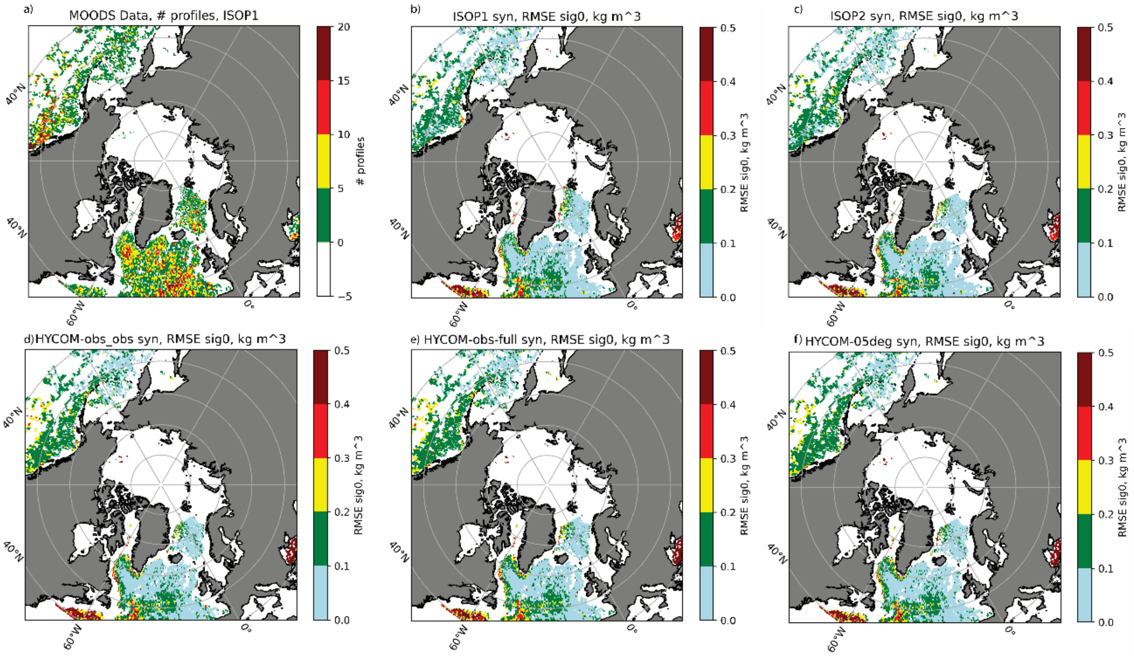

Fig. 9. The synthetic mean RMSE for σ_0 relative to the MOODS in situ profile observations in 1° latitude and longitude bins. The number of observations in each bin is plotted in a). The synthetic test cases are b) ISOP1, c) ISOP2, d) HYCOM-obs-obs, e) HYCOM-obs-full, and f) HYCOM-05deg, as listed in Table 2.

Looking the synthetic profile bias (convention is synthetic - observation) in σ_0 relative to the MOODS data in Figure 10, we see that the ISOP2 synthetics have a slightly larger warm bias in the Gulf of Alaska, compared to the other test cases, including the HYCOM model cases. The bias for the HYCOM-05deg-lastdec, appears to have the smallest overall bias, which is consistent because the last decade of data is closer in time to the validation dataset.

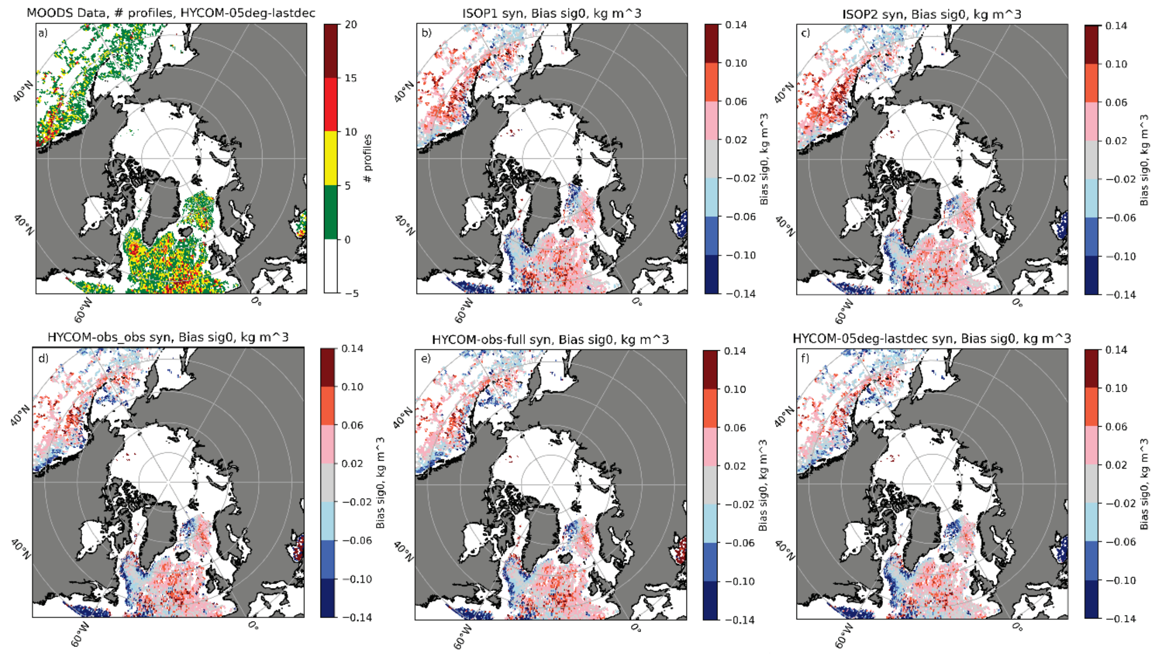

Fig. 10. The synthetic mean BIAS for σ_0 relative to the MOODS in situ profile observations in 1° latitude and longitude bins. The number of observations in each bin is plotted in a). The synthetic test cases are b) ISOP1, c) ISOP2, d) HYCOM-obs-obs, e) HYCOM-obs-full, and f) HYCOM-05deg-lastdec, as listed in Table 2.

To see the difference over depth we plot the T and S RMSE and Bias error as a function of depth in Figure 11. There are nearly 35,000 profiles down to 1000 m, decreasing in number at deep levels. We find over the Arctic Ocean and Subarctic Sea north of 60ºN, that the ISOP2 synthetics have the smallest T RMSE with ISOP1 being a close second. At deeper levels (below roughly 1000m) the GDEM climatology has nearly the same T RMSE as the ISOP2 synthetics. The HYCOM cases have larger T RMSE over most of the water column. The HYCOM-obs-obs case has depth sampling like the ISOP1 case and has the largest RMSE. Notice that the GDEM case has a large negative T bias and T RMSE near the surface, whereas all others have small T errors near the surface. This is because the synthetics all have the profile SST as an input value, thus giving zero error at the surface. The GDEM case, however, does not have this advantage at the surface. In general, all vertical error covariance cases provide a viable database for creating synthetics.

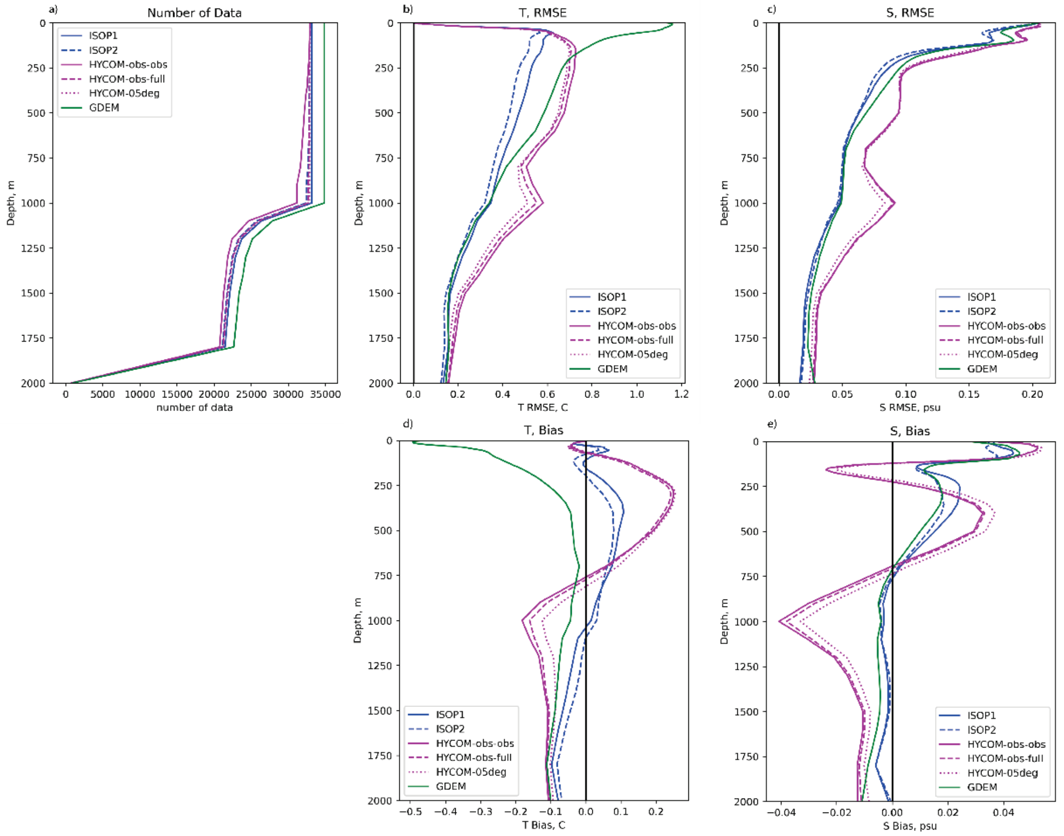

Fig. 11. The synthetic RMSE for (b) temperature and (c) salinity and Bias for (b) temperature and (c) salinity versus depth relative to the MOODS in situ observations for 360 ° of longitude and northward of 60°N. The number of observations versus depth is shown in a) and the synthetic test cases are ISOP1, ISOP2, HYCOM-obs-obs, HYCOM-obs-full, and HYCOM-05deg, listed in the legend.

3.2 Synthetics in OSSE Modeling System

The main goal of this research is to create accurate, data assimilative ocean forecasts for the Arctic and sub-Arctic Seas, northward of 40°N. In Part 1 of this two-paper series, an OSSE framework is utilized for examining the performance of an observational data assimilative ocean forecasting system. The OSSE experiments allow us to test the data assimilative system relative to a simulated ocean called the Nature run. In the OSSEs, the Nature run is a global ocean/sea-ice model that uses the Parallel Ocean Program 2 (POP2) model with the Los Alamos sea ice model 5 (CICE5) coupled together in the Department of Energy (DOE)'s Energy Exascale Earth System Model "HiLAT" framework (E3SMv0-HiLAT) (Hecht et al. 2019). The model's horizontal grid is configured to have nominal resolution close to 8 km at the equator reducing to 4 km at the poles. The initial conditions for POP were taken from the Navy's 1/25° Global Ocean Forecasting System 3.5 (GOFS3.5)

(Metzger et al. 2020) system and the atmospheric forcing used is the Japanese 55-year Atmospheric Reanalysis-driving ocean (JRA55-do) (Tsujino et al. 2018). Further details about the Nature Run can be found in (Fine et al. 2023). The OSSE framework allows experimental test cases using HYCOM , also coupled with CICEv5 (Hunke et al. 2015). The OSSE has a resolution of 1/12^{o} at the equator and is roughly 4 km at the poles. The region used here is known as the Arctic Cap, including all latitudes north of 40^{o}N. Each OSSE was run for one year, starting on January 1, 2017. The initial and boundary conditions are from the GOFS3.5 system (see Part 1 of this paper), and the atmospheric forcing is from JRA55-do.

3.2.1 Synthetics Validation in Regions of Interest

The goal of this analysis is to evaluate synthetics created using numerical ocean model forecast data, vertical error covariances (see Table 1), for SSH data assimilation in a cycling system. We evaluate the synthetics relative to the MOODS data in three regions, one in the Labrador Sea (Figure 12) and two in the Bering Sea (Figure 13 and Figure 14). We first evaluate the synthetic test cases, listed in Table 2, relative to the MOODS data in the five analysis boxes shown in Figure 12d and Figure 13d (also used in Part 1 to evaluate the OSSEs). In the Labrador Sea (Figure 12) we find surprisingly that the GDEM climatology has the smallest RMSE and bias for depths 200m and below. The HYCOM-05deg case has a largest T RMSE near 1000 to 1500 m. At all other depths, the HYCOM-obs-obs case has the largest error. Even given the limited depth sampling of the HYCOM-obs-obs case, the RMSE and Bias errors are still reasonable, compared to the other cases. For salinity, the in-situ cases ISOP1 and ISOP2 have a positive S bias for most of the water column below 250 m, whereas the HYCOM cases tend to have a negative S bias. For the case where the last decade of HYCOM data was used to create the vertical covariances, there is a larger warm bias (Figure 12e) and fresh bias (Figure 12f) in the Labrador Sea. In this region, the Labrador Sea box 2, there are numerous in situ observations for validation and to construct the vertical covariances, thus the observation derived synthetics outperform the model base synthetics. For the next two regions in the Bering Sea, we find that the model-based synthetics are as skillful as the observations-based cases.

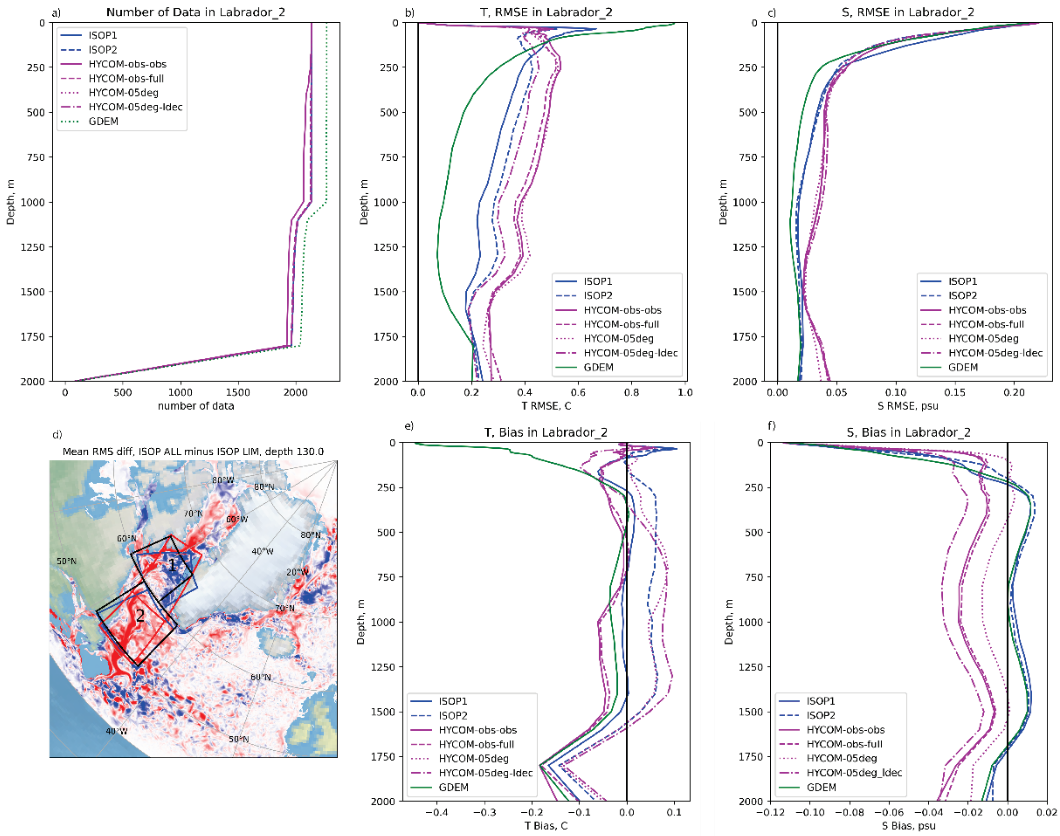

Fig. 12. The synthetic RMSE for (b) temperature and (c) salinity and Bias for (e) temperature and (f) salinity versus depth relative to the MOODS in situ observations for the Labrador Sea in the box labeled "2" in (d). The number of observations versus depth is shown in a) and the synthetic test cases are ISOP1, ISOP2, HYCOM-obs-obs, HYCOM-obs-full, HYCOM-05deg, and HYCOM-05deg_ldec listed in the legend.

In the Bering Sea, box 2 (Figure 13), the synthetic errors are nearly the same for all vertical error covariance test cases. The largest differences occur in T RMSE above 250 m where the HYCOM cases have larger T RMSE and bias above 200 m, where the HYCOM case has a positive T bias and the ISOP1 and ISOP2 cases have a negative T bias. In the Bering Sea, there are much fewer observations for validation and constructing covariance, thus, the model-based synthetics are comparable. The HYCOM-05deg-ldec, case for the last decade of data, is comparable to other HYCOM cases but has the largest salinity bias below 750 m.

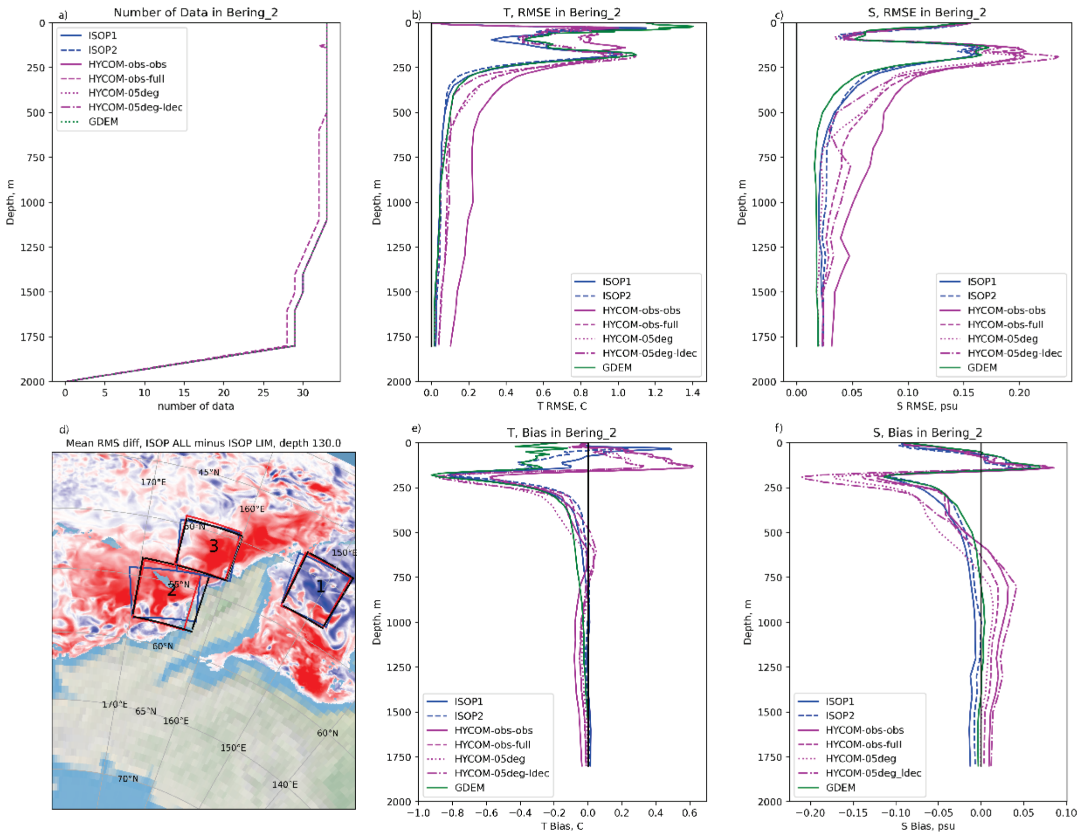

Fig. 13. The synthetic RMSE for (b) temperature and (c) salinity and Bias for (e) temperature and (f) salinity versus depth relative to the MOODS in situ observations for the Bering Sea in the box labeled “2” in (d). The number of observations versus depth is shown in a) and the synthetic test cases are ISOP1, ISOP2, HYCOM-obs-obs, HYCOM-obs-full, HYCOM-05deg, and HYCOM-05deg_ldec, listed in the legend.

In the Bering Sea, box 3 (Figure 14), the synthetic errors are even closer in values compared to box 2 for all vertical error covariance test cases. The largest outlier seems to be the ISOP1 and GDEM cases that have larger T RMSE above 200 m and the GDEM T bias case for not having input SST near the surface. Again, the HYCOM-05deg-ldec, the case for the last decade of data, is comparable to other HYCOM cases but has the largest salinity bias below 750 m.

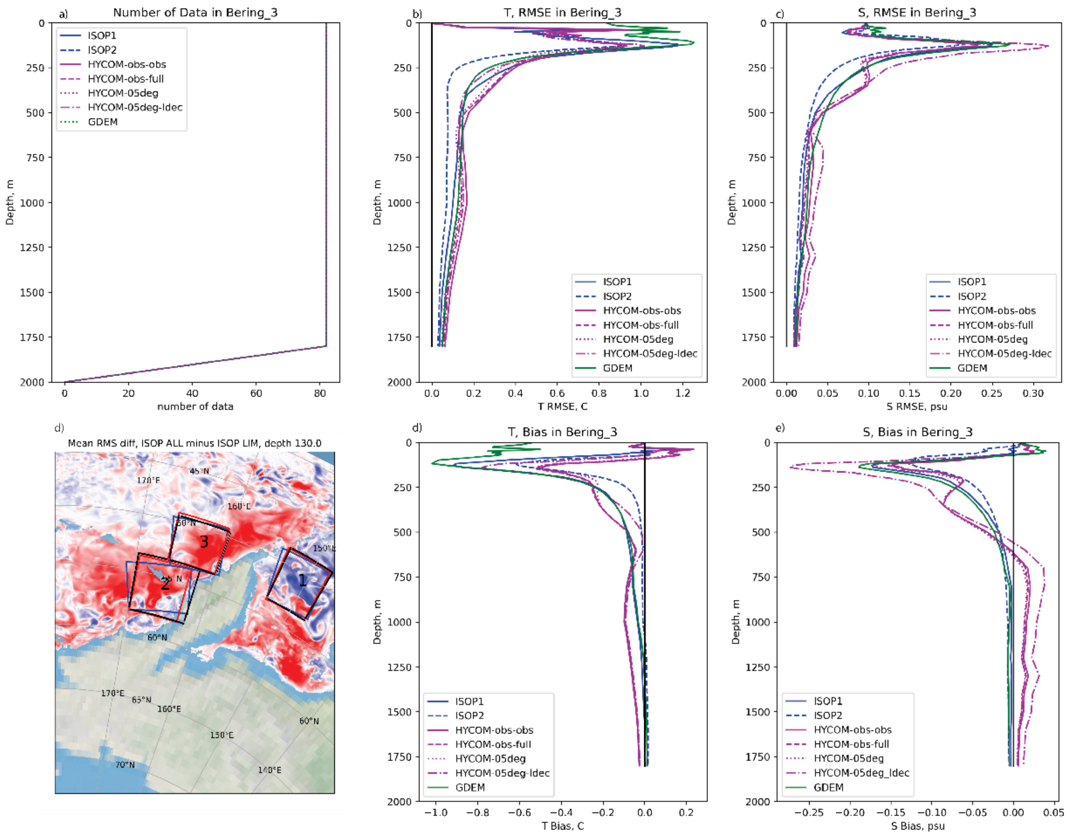

Fig. 14. The synthetic RMSE for (b) temperature and (c) salinity and Bias for (e) temperature and (f) salinity versus depth relative to the MOODS in situ observations for the Bering Sea in the box labeled “3” in (d). The number of observations versus depth is shown in a) and the synthetic test cases are ISOP1, ISOP2, HYCOM-obs-obs, HYCOM-obs-full, HYCOM-05deg, and HYCOM-05deg-ldec listed in the legend.

3.2.2 HYCOM Based Synthetics in OSSE Modeling System

To evaluate the model-based synthetics performance within a cycling data assimilation system, we performed two OSSEs using the framework described in the introduction of section 3.2. The first OSSE case (OSSE-ISOP1) uses ISOP1 synthetics and represents the present operational capability as described in Part 1. The second OSSE case (OSSE-HYCOM-05deg) is new in this manuscript and uses the synthetics derived from HYCOM-05deg vertical error covariances (see Table 1). The data sampling selection includes all available SSH data locations and does not exclude synthetic profiles if the vertical ocean stratification is small (see introduction and Part 1 for detail). Theis new OSSE member was run for one year, starting on January 1, 2017 and the results included here are for one day, December 31st of 2017.

To evaluate the performance of this OSSE experimental test case, we evaluate it relative to the POP2 Nature run in the three boxes of interest used above, one in the Labrador Sea and two in the Bering Sea (Figures 15-17). We compute the spatial average over the box domains for the Nature Run, Climatology, and the OSSE-ISOP1 and OSSE-HYCOM-05deg experiments. In OSSE-ISOP1, the profiles are close to GDEM and the OSSE is not able to emulate the Nature run since SSH data assimilation of synthetics will bring the solution closer toward the synthetics climatology, ISOP1 in this case. In the OSSE-HYCOM-05deg case, the profiles are closer to the Nature run because the synthetics represent the time evolution of the global non-assimilative HYCOM model evolves away from the GDEM initial conditions (Chassignet et al. 2020) as it is the case for the POP Nature run. In box 2 of the Labrador sea, OSSE-HYCOM-05deg is closer to OSSE-ISOP1 and GDEM than to the Nature run (Figure 15). In box 2 and 3 of the Bering Sea, OSSE-HYCOM-05deg is closer to the Nature run as both HYCOM and the Nature run are not able to represent the temperature inversion present in this region (Figure 16 and 17). In this case, the GDEM climatology is far from the POP2 Nature run in the Bering Sea.

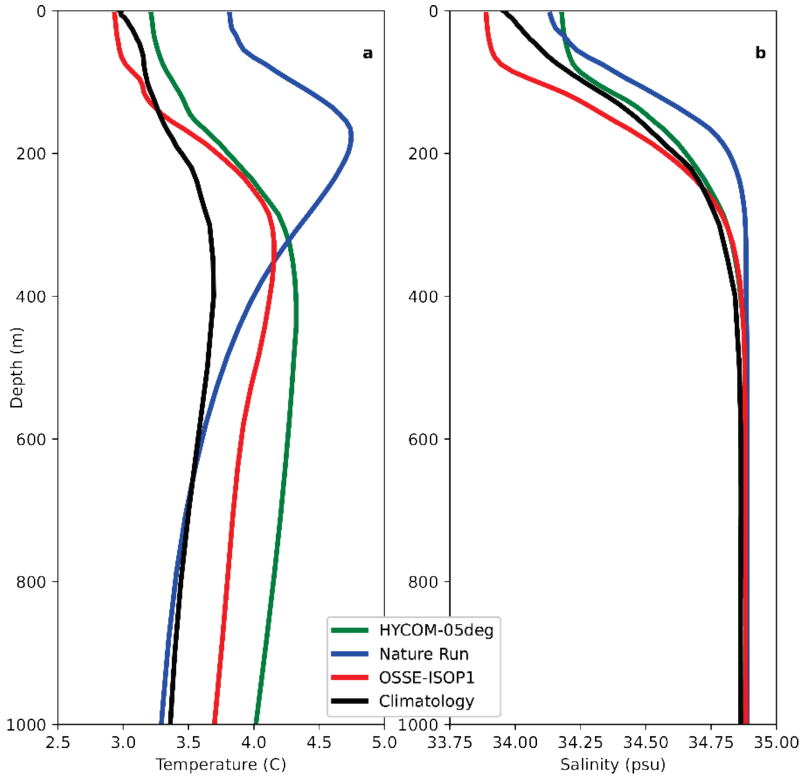

Fig. 15. The spatial average, in the Labrador Sea in box 2 (see Figure 12d), versus depth of a) temperature and b) salinity for OSSE member OSSE-HYCOM-05deg (green line) utilizing the HYCOM-05deg vertical error covariance and OSSE-ISOP1 (red line) to create synthetics. The blue line is the Nature run and the black line is GDEM climatology. The results here are for one day, December 31st of 2017.

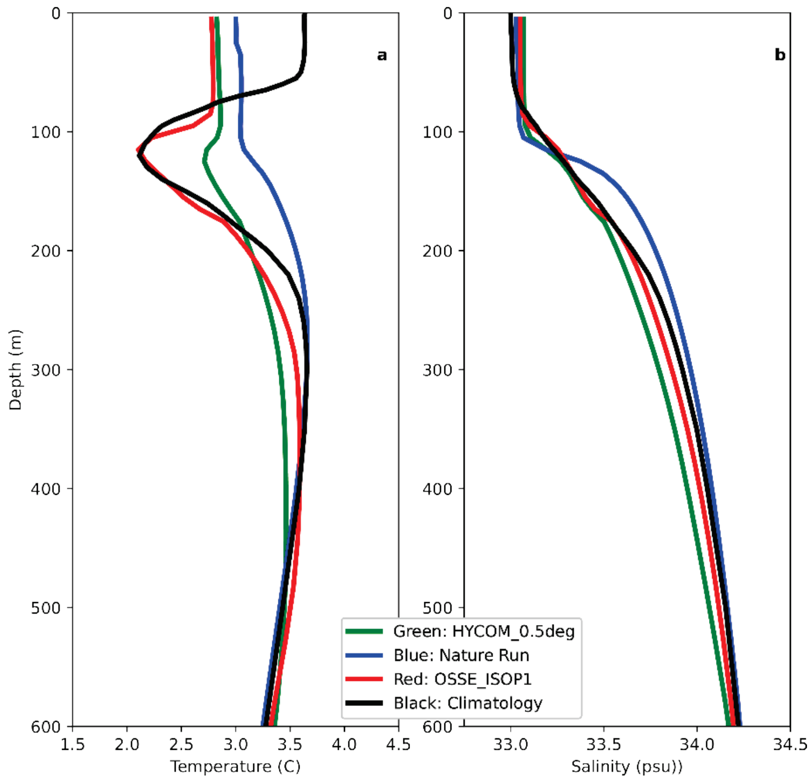

Fig. 16. The spatial average, in the Bering Sea in box 2 (see Figure 12d), versus depth of a) temperature and b) salinity for OSSE member OSSE-HYCOM-05deg (green line) utilizing the HYCOM-05deg vertical error covariance and OSSE-ISOP1 (red line) to create synthetics. The blue line is the Nature run and the black line is climatology.

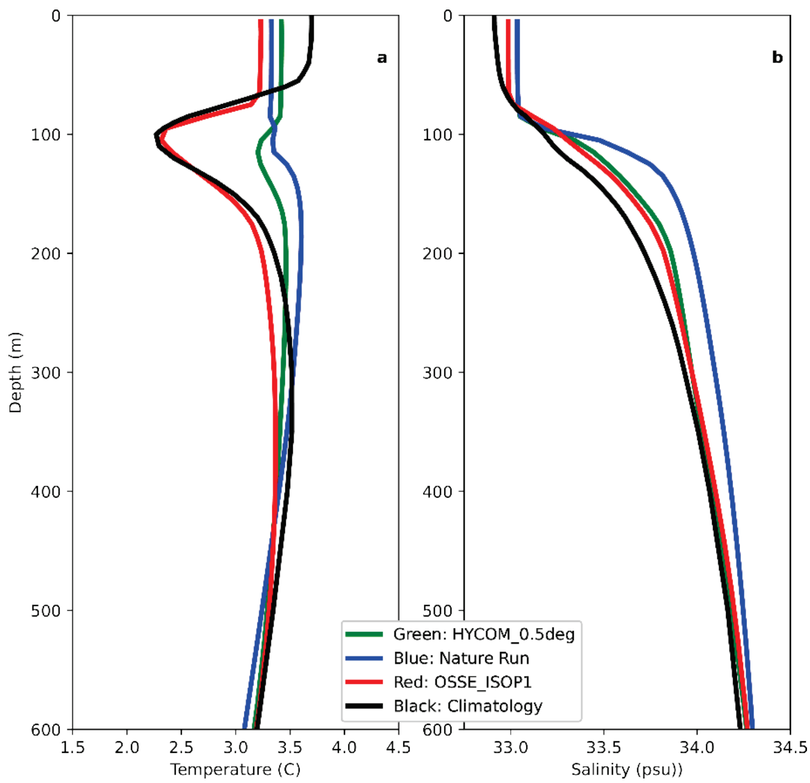

Fig. 17. The spatial average, in the Bering Sea in box 3 (see Figure 12d), versus depth of a) temperature and b) salinity for OSSE member OSSE-HYCOM-05deg (green line) utilizing the HYCOM-05deg vertical error covariance and OSSE-ISOP1 (red line) to create synthetics. The blue line is the Nature run and the black line is climatology.

3.3 Analysis of Synthetic Errors on T vs. S Diagrams

To evaluate the effectiveness of limiting the use of synthetics at high latitude based on stratification (see the Introduction and Figure 2), we compute histograms, weighted by density RMS error on T versus S diagrams. In Figure 18, there are three types of two-dimensional (2D) histograms. In Figure 18a, we show the 2D histogram of the number of values in each bin. In Figure 18b, we show the 2D histogram of the number of values in each bin, weighted by density RMS error. In Figure 18 c, d, and e, we show the ratio of the two histograms. The result provides an estimate of the rate of error in each bin. Because the stratification test is computed from the synthetics as the temperature difference between the surface and 1000 m, we create bins that cover the difference in T and S from the surface to 1000 m. For T, there are 50 evenly spaced bins from -5^{o}C to 15^{o} C and for S, there are 50 evenly spaced bins from -5 psu to 1.1 psu (Figure 18). The histogram in Figure 18a shows the number of profiles with the corresponding T and S difference between 0 and 1000 m depth. Figure 18b weights each one by the RMS Error with depth of the profile σ_0. In Figure 18, c, d, and e, we have the ratio of a and b for the ISOP1, ISOP2, and HYCOM Last Decade test cases.

We can see that there are areas where the difference in temperature from the surface to 1000 m depth has relatively good synthetics for low T stratification. The cutoff in the present system is 3^{o}C (see Part 1). In this case, the region in these plots on the y-axis from -3^{o}C to 3^{o}C, would be eliminated (green lines in Figure 18c). Clearly, this threshold is too strict and often wrong, as low T stratification is not a good indicator of synthetics quality. Instead, salinity stratification may be a better indicator, which we explore next.

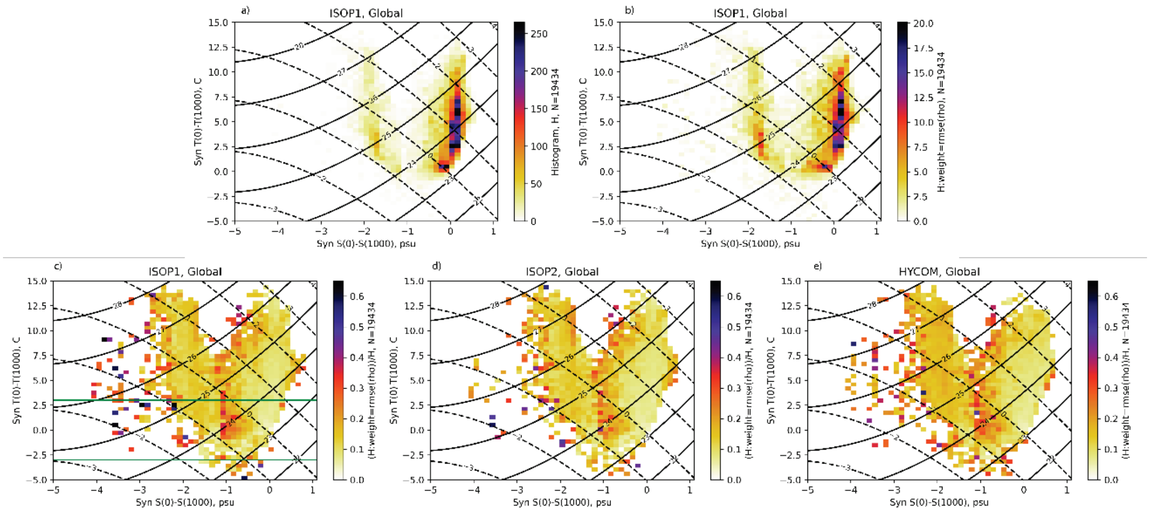

Fig. 18. Histograms of the a) number of profiles, b) number of profiles weighted by the density RMS Error over depth of the synthetics, and the ratio of a) and b) for the c) ISOP1, d) ISOP2, and e) HYCOM Last Decade test cases. Panels represent the rate of error for the synthetics. The histogram is sorted in bins of the difference from the surface to 1000 m for T and S. For T, there are 50 evenly spaced bins from -5^{o}C to 15^{o} C and for S, there are 50 evenly spaced bins from -5 psu to 1.1 psu. The solid contour lines are surface reference potential density σ_θ and the dashed contour lines are potential spiciness referenced to the surface (McDougall and Krzysik 2015).

Because the ocean at 1000 m is relatively unchanging compared to the upper ocean, we can ignore the 1000 m synthetic values for evaluating the veracity of the synthetics. If we consider the two-dimensional histograms using just the surface values with 50 evenly spaced bins of temperature from -1.8^{o} C to 20.0^{o} C and 50 evenly spaced bins of salinity from 30.25 psu to 35.9 psu, the result is in Figure 19. Thus, the primary variable for evaluating the skill of synthetics are the surface values, which are controlled primarily by the input SST and climatological S, since surface salinity is not an input. The synthetic values of T and S at 1000 m do not change enough for them to be a major factor. In Figure 20, we show the same calculation in each of the regions of interest for the Labrador (see Figure 12) and Bering (see Figure 13) Seas. For the Bering Sea, there are not many profiles, but the synthetics have relatively good performance relative to other regions.

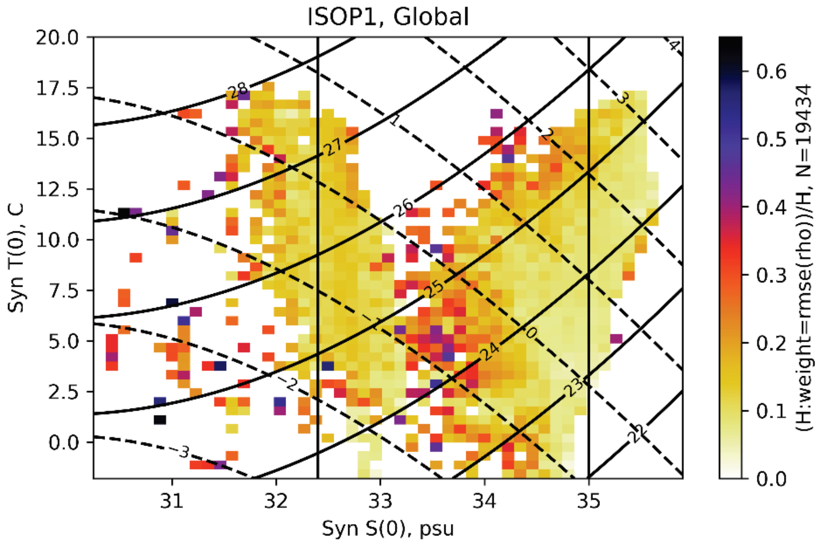

Fig. 19. Histograms of the ratio of the number of profiles to the number of profiles weighted by the density RMS Error over depth of the synthetics for the ISOP1 test case. The bins are sorted by the surface T and S values of the synthetic profiles with 50 evenly spaced bins of temperature ranging from -1.8ºC to 20.0ºC and 50 evenly spaced bins of salinity ranging from 30.25 psu to 35.9 psu. The contour lines are the same as in Figure 18. The straight vertical black lines at 32.4 psu and 35.0 psu..

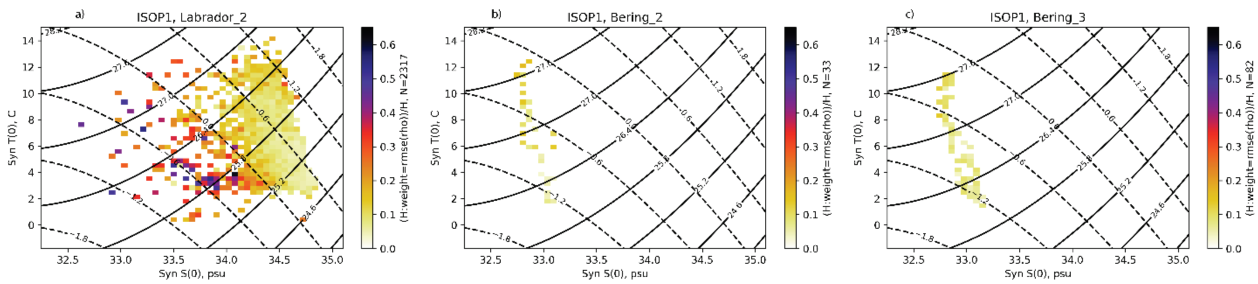

Fig. 20. Histograms of the ratio of the number of profiles to the number of profiles weighted by the density RMS Error over depth of the synthetics for the ISOP1 test case. The bins are the same as those in Figure 19. In a) we have the Labrador Sea box 2, b) the Bering Sea box 2, and c) the Bering Sea box 3. The contour lines are the same as in Figure 18.

3.4 Determine T/S areas of synthetics quality

To determine when synthetics are skillful, the observation error for the synthetics can be determined by only the surface values of the synthetics. The rule seems to be dependent on the region of the ocean. The T versus S areas where synthetics are more skillful is different in the North Atlantic compared to the North Pacific. In fact, it seems that the skill of the synthetics depends mostly on salinity. If we simply select a salinity value of 35ºC for the Atlantic Ocean and 32.4ºC for the Pacific Ocean, we see that many of the synthetics are skillful near these values (see Figure 19). This is a curious finding given the fact that surface salinity is not an input parameter for making synthetics (see Section 2 and the Appendix). Future systems should have the error level associated with the synthetic be dependent on surface salinity.

Another potential criterion to determine synthetic error levels is the deviation from the climatological T value at the location of the synthetic. Since, there is no input S for creating synthetics, the surface S for the salinity is very close to the climatological value. The T value, however, varies according to the input SST values. Evaluating this relative to the climatological value reveals an interesting relationship (Figure 21). The synthetics have a higher rate of error for input SST values that are far from the climatological value. This suggests that synthetics are more accurate when the SST is close to the climatology value. Thus, the vertical covariances are most representative to the observed ocean.

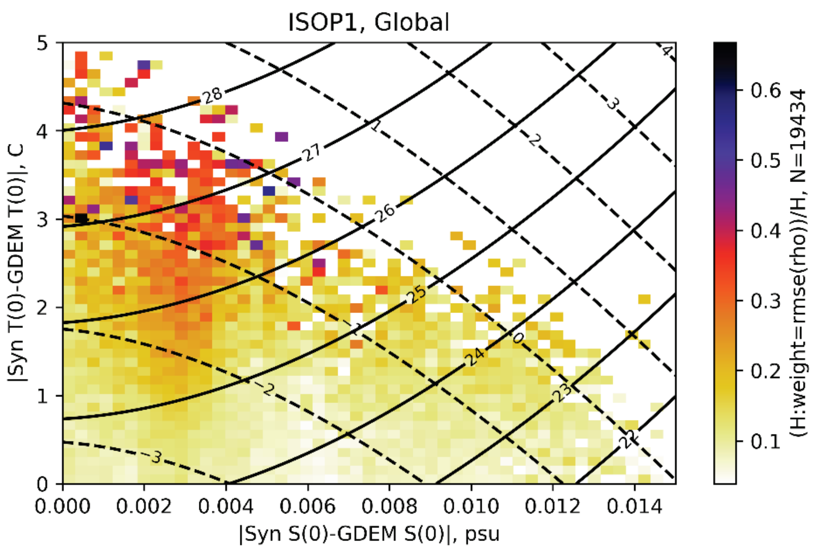

Fig. 21. Histograms of the rate of error computed as ratio of the number of profiles to the number of profiles weighted by the density RMS Error over depth of the synthetics for the ISOP1 test case. The histogram is sorted in bins of the difference of the synthetic from GDEM climatology. For T, there are 50 evenly spaced bins ranging from 0ºC to 5º C and for S, there are 50 evenly spaced bins ranging from 0 psu to 0.014 psu. The contour lines are the same as in Figure 18.

4. Conclusions

This paper describes research aimed at creating accurate, data assimilative ocean forecasts for the Arctic and sub-Arctic Seas. A key approach is the use of model data as a substitute for *in situ* observed ocean vertical error covariances of temperature and salinity in a data assimilative ocean forecasting system. We also evaluate usage of SSHA data assimilation via synthetics at high latitude, where this method has historically been restricted.

Using the model data, we focus on five different versions of the covariances, two that come from in situ observations and three derived from HYCOM ocean model simulations. The advantage of using model data is the uniform coverage of the global ocean in space and time, including at high latitude where in situ observations are sparse. The results of this analysis suggest that model data is a suitable replacement for where and when in situ observations are not present. All cases present a viable option for application in an operational ocean data assimilation system. In general, the observation based vertical covariances perform better, in making synthetics, compared to the model base covariances. In regions of the ocean where there are few in situ observations, such as the Bering Sea, the model based covariances perform similarly to the observation based covariances. For the case where the last decade of HYCOM data was used to create the vertical covariances, there is a larger warm bias and fresh bias in the Labrador Sea. In the Bering Sea, the last decade of data increased the salinity bias below 750 m.

As described in section 2.3, the model derived covariance test cases have a slight disadvantage compared to the in situ derived covariance cases. The disadvantage is due to the derivation of the climatological mean steric height values. In the in situ observation test cases, ISOP1 and ISOP2, the in situ derived monthly climatological and annual mean steric height data is consistent with the in situ derived vertical error covariances. In the model derived HYCOM test cases, the same in situ derived annual mean steric height data is used. The monthly climatological mean steric height data, however, comes from the model data itself. This inconsistency is minor since the monthly climatological mean anomaly is separate from the annual mean anomaly. The system equates the anomalies, not the total steric height. Thus, this inconsistency is likely to have a small or potential negligible impact.

A motivating factor for using model data as a source of ocean covariances is the time and space sampling, which is superior to that of available in situ observations. Because of the limited observations, particularly at high latitude, present Navy ocean data assimilation systems restrict the use of synthetic profiles at high latitudes (see Part 1). A goal of this research is to extend synthetic usage to higher latitude using model derived vertical error covariances. The present analysis shows that model derived synthetics perform accurately in the Bering and Labrador Seas. In the central Arctic, however, there is a negative cross-correlation between T and S in the ISOP2 dataset, whereas the HYCOM-obs-obs and the HYCOM_05deg cases have a positive cross-correlation, suggesting that the HYCOM solution may not work correctly there. For this evaluation, there was no data that satisfied the criteria requiring data to extend down to 1000 m in the central Arctic Ocean and thus we were unable to evaluate the system there. In addition, Baffin Bay is another region where the HYCOM data has an opposite T/S cross-correlation to that of the ISOP1 data set.

Since the inputs for making synthetics include SST, SSH and MLD, salinity is only controlled by the error covariances and not through inputs. For this reason, the salinity errors were relatively equal among the test cases. In the Labrador Sea, the salinity bias is opposite for the in situ derived versus the HYCOM model derived test cases.

In corroboration with the findings in the companion paper (Part 1), the accuracy of the climatological mean structure used in the construction of the synthetics is crucial to the results, as shown in the OSSE experiment. Thus, inaccurate climatological mean state in the synthetic database will inject those inaccuracies in the model prediction.

A key finding of this research is the dependence of the synthetics skill is most closely related to the surface salinity of the synthetic. Since there is no salinity input for creating synthetics, the surface salinity of the synthetics is nearly identical to climatology. Thus, maps of good synthetics skill can be determined from maps of climatology surface salinity. This finding suggests that observations of salinity, if incorporated into the system, could substantially improve the accuracy of synthetics.

For future applications, the model derived solution could be used everywhere except potentially the central Arctic and Baffin Bay. Due to few available in situ observations for validation, however, we are unable to validate the system in those locations. This method would be particularly useful in regions with few data such as the central Arctic Ocean, Sea of Okhotsk or Baffin Bay, provided the model solution is correct.

Acknowledgments.

This work was performed with funding from the National Ocean Partnership Program, under a project entitled "Arctic Observing System Simulation Experiments (OSSEs) within the ONR/Navy Global Ocean Forecasting System (GOFS) and Earth System Prediction Capability (ESPC) frameworks" led by Florida State University, project number N00014-19-12674. In addition to the NOPP funding, J. McClean (SIO/UCSD) was supported by Office of Naval Research (ONR) award number N00014-24-12541. The Naval Research Laboratory also received additional funding from ONR award number 73-1D57-13-5 and program manager Scott L. Harper. The Nature Run used in this study was produced at the U.S. Army Engineer Research and Development Center (ERDC) DoD Supercomputing Resource Center (DSRC) using computing resources from the Department of Defense (DoD) High Performance Computing Modernization Program (HPCMP). This paper is contribution NRL/PO/7320-25-6787 and has been approved for public release.

Data Availability Statement.

The authors do not have permission to release the data and software to the public.

APPENDIX

The 1D synthetic model formulation

The system for constructing synthetic profiles from surface observations of sea surface temperature, $\tilde{T}_1$ and height anomaly, $\delta\tilde{h}$, has a dynamic layer constrained by empirically derived vertical covariances (Helber et al. 2013). The cost function, to create one synthetic profile at a location, is given by

$$\begin{aligned}
J = &\left(\delta\mathbf{x}^{(clim)}\right)^T \mathbf{B}^{-1}\left(\delta\mathbf{x}^{(clim)}\right) + \left(\delta\mathbf{d}^{(\mathrm{clim})}\right)^T \left(\mathbf{B}^{(\mathbf{d})}\right)^{-1}\left(\delta\mathbf{d}^{(\mathrm{clim})}\right) \\
&+\left(\delta\mathbf{x}^{(eof)}\right)^T \mathbf{V}^{-1}\left(\delta\mathbf{x}^{(eof)}\right) + \left(\delta\mathbf{d}^{(eof)}\right)^T \left(\mathbf{V}^{(\mathbf{d})}\right)^{-1}\left(\delta\mathbf{d}^{(eof)}\right) \\
&+\left(\delta\tilde{T}_1^{(obs)}\right)\left(R^{(SST)}\right)^{-1}\left(\delta\tilde{T}_1^{(obs)}\right) + \left(\mathbf{L}\delta\mathbf{x}^{(clim)} - \delta\tilde{h}^{(\mathrm{clim})}\right)\left(R^{(SSHA)}\right)^{-1}\left(\mathbf{L}\delta\mathbf{x}^{(clim)} - \delta\tilde{h}^{(\mathrm{clim})}\right).
\end{aligned} \tag{A1}$$

The first term involves the anomaly of the synthetic solution from the climatological profile, for the month, at the profile's location given by

$$\delta \mathbf{x}^{(clim)} = \mathbf{x} - \mathbf{x}^{(clim)}, \qquad \text{(A2)}$$

where

$$\mathbf{x} = \begin{bmatrix} T_{k_{mld}} & T_{k_{mld}+1} & \cdots & T_{nz} & S_{k_{mld}} & S_{k_{mld}+1} & \cdots & S_{nz} \end{bmatrix}, \qquad \text{(A3)}$$

and T and S are the synthetic temperatures and salinity, respectively, at depths k_{mld}, $k_{mld}+1$, $k_{mld}+2$, etc. down to the last depth grid nz, where k_{mld} is the index of the analysis grid below the input mixed layer depth (MLD). Now $\mathbf{x}^{(clim)}$ has the same form but with climatological values

$$\mathbf{x}^{(clim)} = \begin{bmatrix} T^{(clim)}_{k_{mld}} & T^{(clim)}_{k_{mld}+1} & \cdots & T^{(clim)}_{nz} & S^{(clim)}_{k_{mld}} & S^{(clim)}_{k_{mld}+1} & \cdots & S^{(clim)}_{nz} \end{bmatrix}. \qquad \text{(A4)}$$

The second term involves the anomaly of the synthetic solution vertical difference from the climatological profile vertical difference, for the month, at the profile's location given by

$$\delta \mathbf{d}^{(clim)} = \mathbf{d} - \mathbf{d}^{(clim)} \qquad \text{(A5)}$$

where

$$\mathbf{d} = \begin{bmatrix} T_{k_{mld}+1} - T_{k_{mld}} & T_{k_{mld}+2} - T_{k_{mld}+1} & \cdots & T_{nz} - T_{nz-1} & \cdots \\ S_{k_{mld}+1} - S_{k_{mld}} & S_{k_{mld}+2} - S_{k_{mld}+1} & \cdots & S_{nz} - S_{nz-1} & \end{bmatrix} \qquad \text{(A6)}$$

and $\mathbf{d}^{(clim)}$ has the same form but with climatological values

$$\mathbf{d}^{(clim)} = \begin{matrix} [T^{(clim)}_{k_{mld}+1} - T^{(clim)}_{k_{mld}} & T^{(clim)}_{k_{mld}+2} - T^{(clim)}_{k_{mld}+1} & \cdots & T^{(clim)}_{nz} - T^{(clim)}_{nz-1} & \cdots \\ S^{(clim)}_{k_{mld}+1} - S^{(clim)}_{1k_{mld}} & S^{(clim)}_{k_{mld}+2} - S^{(clim)}_{k_{mld}+1} & \cdots & S^{(clim)}_{nz} - S^{(clim)}_{nz-1}] & \end{matrix} \qquad \text{(A7)}$$

The background vertical error covariance, for this location and month, is

$$\mathbf{B} = \mathbf{UCU}, \qquad \text{(A8)}$$

where the climatological standard deviation is $\mathbf{U}$ and climatologically derived correlation is $\mathbf{C}$. We compute the analogous background error covariance for the vertical difference of the synthetic values given by

$$\mathbf{B}^{(\mathbf{d})} = \mathbf{U}^{(\mathbf{d})}\mathbf{C}^{(\mathbf{d})}\mathbf{U}^{(\mathbf{d})}. \qquad \text{(A9)}$$

where the climatological standard deviation is $\mathbf{U}^{(\mathbf{d})}$ and climatologically derived correlation is $\mathbf{C}^{(\mathbf{d})}$, computed from vertical differences in T and S as in equation (A7). The Navy's Master Oceanographic Observation Data Set (MOODS) (Bauer 1985; Teague 1987) is the in situ profile database used to create $\mathbf{B}$ and $\mathbf{B}^{(\mathbf{d})}$. We separate the correlations into four components such that

$$\mathbf{C} = \begin{bmatrix} \mathbf{C}^{(T-T)} & \mathbf{C}^{(T-S)} \\ \mathbf{C}^{(T-S)} & \mathbf{C}^{(S-S)} \end{bmatrix} \text{ and } \mathbf{C}^{(d)} = \begin{bmatrix} \mathbf{C}^{(\mathbf{d})(T-T)} & \mathbf{C}^{(\mathbf{d})(T-S)} \\ \mathbf{C}^{(\mathbf{d})(S-T)} & \mathbf{C}^{(\mathbf{d})(S-S)} \end{bmatrix}, \qquad \text{(A9)}$$

where $\mathbf{C}^{(T-T)}$, $\mathbf{C}^{(S-S)}$, $\mathbf{C}^{(\mathbf{d})(T-T)}$ and $\mathbf{C}^{(\mathbf{d})(S-S)}$ are the auto-correlations for T and S and $\mathbf{C}^{(T-S)}$, $\mathbf{C}^{(S-T)}$, $\mathbf{C}^{(\mathbf{d})(T-S)}$, and $\mathbf{C}^{(\mathbf{d})(S-T)}$ are the cross-correlations for T and S and the transposes for each. Figure 3 shows the vertical correlation $\mathbf{C}$ and Figure A 1 shows the vertical difference correlations $\mathbf{C}^{(\mathbf{d})}$. The data in Figure 3 and Figure A 1 are valid at a location in the Lofoten Basin within the Norwegian Sea.

The terms on the 2nd line of equation (1) constrain the synthetic profile to the reduced EOF mode representation of the climatological vertical profile. Those terms are normalized by the climatological variances give by $\mathbf{V}$ and $\mathbf{V}^{(d)}$. For computational efficiency and to reduce data storage, the full correlations, $\mathbf{C}$, for the global ocean at 1/2° resolution represented by a six-mode Jordan decomposition given by (e.g. Strang 2006)

$$\mathbf{B} = \mathbf{U}\mathbf{\Gamma}\mathbf{\Lambda}\mathbf{\Gamma}^T\mathbf{U}, \qquad \text{(A10)}$$

where $\mathbf{\Lambda}$ is a diagonal matrix with elements, λ_i, equal to the singular values of $\mathbf{C}$. The columns of the orthogonal matrix, $\mathbf{\Gamma}$, are the combined T and S eigenvectors, γ_i, of $\mathbf{C}$. From the EOF decomposition, we construct amplitudes given by

$$\mathbf{a} = \mathbf{\Gamma}^T\mathbf{U}^{-1}\left(\mathbf{x} - \mathbf{x}^{(\mathrm{clim})}\right) \qquad \text{(A11)}$$

and for the vertical difference

$$\mathbf{a}^{(d)} = \mathbf{\Gamma}^{(d)T}\mathbf{U}^{(d)-1}\left(\mathbf{d} - \mathbf{d}^{(\mathrm{clim})}\right) \tag{A12}$$

Using 6 modes of eigenvectors and eigenvalues, the 1st term on the 2nd line of equation 1 has

$$\delta\mathbf{x}^{(eof)} = \mathbf{U}\mathbf{\Gamma}^{(6)}\mathbf{a}^{(6)}. \tag{A13}$$

Similarly, for the vertical difference, constraint we have

$$\delta\mathbf{d}^{(eof)} = \mathbf{U}^{(d)}\mathbf{\Gamma}^{(d:6)}\mathbf{a}^{(d:6)}. \tag{A14}$$

The first term on the third line of equation (A1) is the SST term, which has

$$\delta\tilde{T}_1^{(obs)} = T_1 - \tilde{T}^{(SST)} \tag{A15}$$

where T_1 is the first level synthetic temperature in equation 1 and $\tilde{T}^{(SST)}$ is the input observed sea surface temperature (SST) value. The $R^{(SST)}$ in equation 1 it the error estimate for SST, which include representation errors, not just instrument error.

From equation A3, we see that the solution is solved from the depth level just below the MLD. Thus, there is a procedure for translating the SST in equation 15, down to the depth level k_mld (Helber et al. 2013). The last term in equation (A1) is the constraint of the synthetic profiles to the observed sea surface height anomaly $\delta\tilde{h}$. This input value differs from the variable in equation (1), $\delta\tilde{h}^{(\mathrm{clim})}$ such that

$$\delta\tilde{h}^{(\mathrm{clim})} = \delta\tilde{h} + h^{(annual)} - h^{(\mathrm{clim})}, \tag{A16}$$

where $h^{(annual)}$ is the steric height referenced to 1000 m, as computed from historical in situ profile observations. The last variable, $h^{(\mathrm{clim})}$ is the climatological monthly steric height referenced to 1000 m, as computed from historical in situ profile observations. Thus, $\delta\tilde{h}^{(\mathrm{clim})}$ is the deviation of the observed sea surface height from the climatological steric height. Because the input observed sea surface height anomaly operationally will come from satellite altimetry observations, this anomaly is relative to a long-term altimetry mean. Thus, our approach assumes that the actual full sea surface height is approximately

$$\tilde{h} \cong \delta\tilde{h} + h^{(annual)}. \tag{A17}$$

The notation, $\mathbf{L}\delta\mathbf{x}^{(\mathrm{clim})}$, in the last term of equation (1) represents an application of the linearized operator $\mathbf{L}$, which computes the anomaly of the synthetic steric height referenced to 1000 m relative to climatology for the month. Thus, $\mathbf{L}\delta\mathbf{x}^{(clim)} - \delta\tilde{h}^{(\mathrm{clim})}$ is the difference of the synthetic minus the observed anomaly from climatology. The cost function form of this term (last term in (1)) includes $R^{(SSHA)}$, which is the estimated error variance for $\delta\tilde{h}$.

Note, the solution obtained by minimizing the cost function (equation A1) are synthetic values of T and S that represent an estimate for the time and location of the observed surface values. Thus, the steric height of the resulting synthetic will match $\delta\tilde{h} + h^{(annual)}$ from equation (A11) most closely.

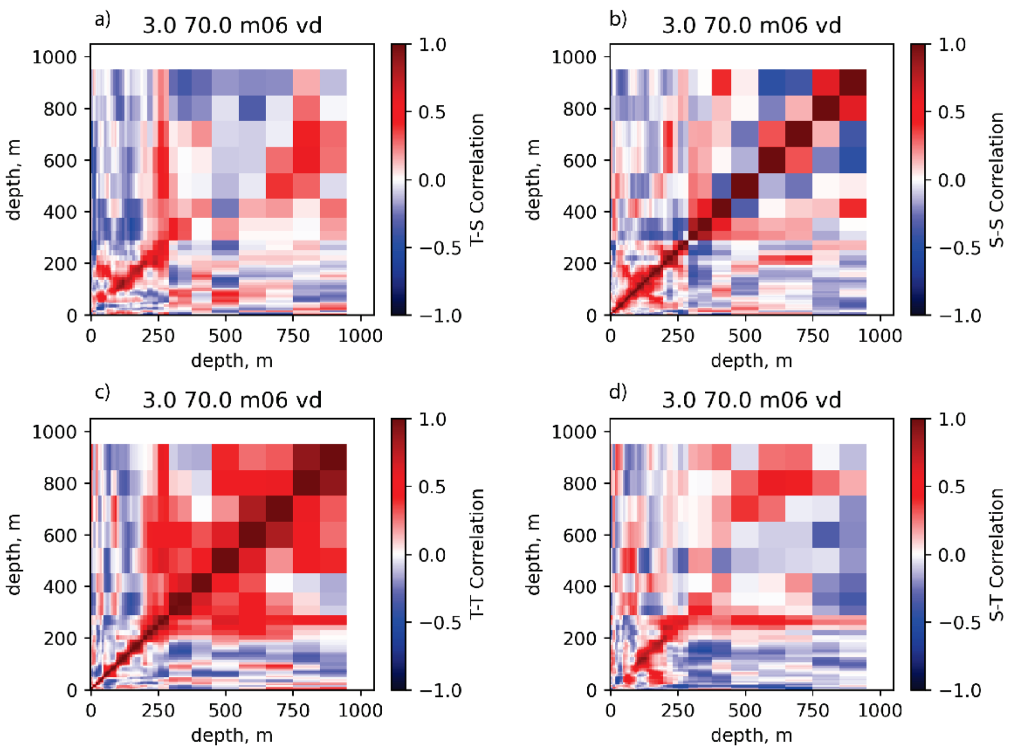

Fig. A1. The vertical difference correlations for T and S at 3E, 70N. The auto-correlations for T and S are along the diagonal in panels b and c. The off diagonal correlations for S with T and T with S are in panels a and

d. Since the correlations go from 0 to 1000 m, the x and y axes cover the same depths. The block structure indicates there are 47 depth levels in the upper 1000 m, where the block indicates depth bins that get larger with depth. The vertical difference correlation $\mathbf{C}$ components a) $\mathbf{C}^{(d)(T-S)}$, b) $\mathbf{C}^{(d)(S-S)}$, c) $\mathbf{C}^{(d)(T-T)}$, and $\mathbf{C}^{(d)(S-T)}$ for the location 0, 70N in the high north Atlantic.

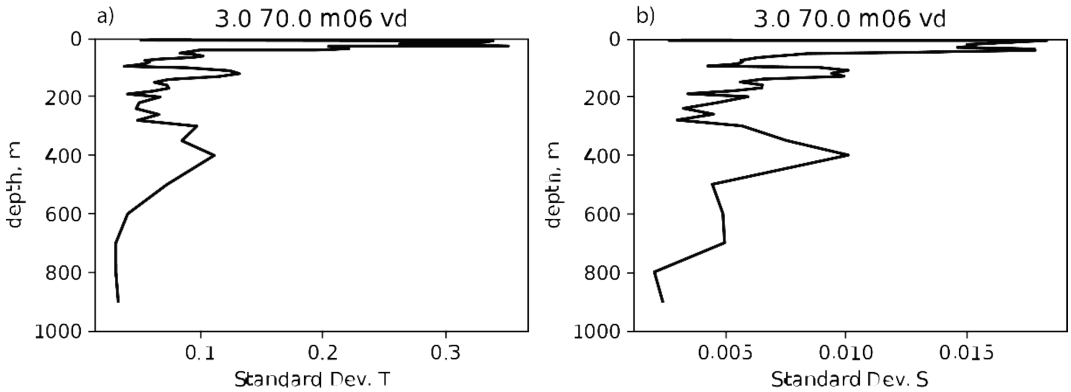

Fig. A2. The vertical difference standard deviation profile for T and S for June at 3E, 70N, corresponding with the correlations shown in Figure A 1.

REFERENCES

Bauer, R. A., 1985: Functional description Master Oceanographic Observation Data Set (MOODS).

Bleck, R., 2002: An oceanic general circulation model framed in hybrid isopycnic-Cartesian coordinates. *Ocean Modelling*, **4,** 55-88.

Carnes, M., R. W. Helber, C. N. Barron, and J. M. Dastugue, 2010: Valication Test Report for GDEM4. Memorandum Report, 65 pp.

Chassignet, E. P., L. T. Smith, G. R. Halliwell, and R. Bleck, 2003: North Atlantic Simulations with the Hybrid Coordinate Ocean Model (HYCOM): Impact of the vertical coordinate choice, reference pressure, and thermobaricity. *JOURNAL OF PHYSICAL OCEANOGRAPHY*, **33,** 2504-2526.

Chassignet, E. P., and Coauthors, 2020: Impact of horizontal resolution on global ocean-sea ice model simulations based on the experimental protocols of the Ocean Model Intercomparison Project phase 2 (OMIP-2). *GEOSCIENTIFIC MODEL DEVELOPMENT*, **13,** 4595-4637.

Douglass, E. M., R. W. Helber, J. L. McClean, A. Bozec, E. Chassignet, and A. J. Wallcraft, 2025: Improving High-Latitude Sea Surface Height Data Assimilation: Part I Selective Synthetics. *Journal of Atmospheric and Oceanic Technology*.

Fine, E. C., J. L. McClean, D. P. Ivanova, A. P. Craig, A. J. Wallcraft, E. P. Chassignet, and E. C. Hunke, 2023: Arctic ice-ocean interactions in an 8-to-2 kilometer resolution global model. *OCEAN MODELLING*, **184**.

Hecht, M., and Coauthors, 2019: E3SMv0-HiLAT: A Modified Climate System Model Targeted for the Study of High-Latitude Processes. *J. Adv. Model. Earth Syst.*, **11,** 2814-2843.

Helber, R. W., T. L. Townsend, C. N. Barron, J. M. Dastugue, and M. R. Carnes, 2013: Validation Test Report for the Improved Synthetic Ocean Profile (ISOP) System, Part I: Synthetic Profile Methods and Algorithm. Memorandum Report NRL/MR/7320--13-9364, 120 pp.

Helber, R. W., and Coauthors, 2023: Ocean drifter velocity data assimilation, Part 1: Formulation and diagnostic results. *Ocean Modelling*, **183**.

Hunke, E. C., W. Lipscomb, H., A. K. Turner, N. Jeffery, and S. Elliot, 2015: CICE: the Los Alamos Sea Ice Model Documentation and Software User's Manual Version 5.1, 116 pp.

McDougall, T. J., and O. A. Krzysik, 2015: Spiciness. *Journal of Marine Research*, **73,** 141-152.

Metzger, E. J., and Coauthors, 2014: US Navy Operational Global Ocean and Arctic Ice Prediction Systems. *Oceanography*, **27,** 32-43.

Metzger, E. J., and Coauthors, 2020: Validation Test Report for the Global Ocean Forecast System 3.5 – 1/25º HYCOM/CICE with Tides.

Miyazawa, Y., and Coauthors, 2009: Water Mass Variability in the Western North Pacific Detected in a 15-Year Eddy Resolving Ocean Reanalysis. *J. Oceanogr.*, **65,** 737-756.

Oke, P. R., G. B. Brassington, D. A. Griffin, and A. Schiller, 2008: The Bluelink ocean data assimilation system (BODAS). *Ocean Modelling*, **21,** 46-70.

Raj, R. P., and Coauthors, 2020: Interaction Between Mesoscale Eddies and the Gyre Circulation in the Lofoten Basin. *J. Geophys. Res.-Oceans*, **125**.

Strang, G., 2006: *Linear Algebra and Its Applications.* 4th ed. Thomson, 488 pp.

Teague, W. J., Molinelli, E. J. and Carron, M. J., 1987: A new system for management of the "Master Oceanographic Observation Data Set" (MOODS). *EOS Transactions*, AGU, 558-559.

Thoppil, P. G., and Coauthors, 2021: Ensemble forecasting greatly expands the prediction horizon for ocean mesoscale variability. *COMMUNICATIONS EARTH & ENVIRONMENT*, **2**.

Tsujino, H., and Coauthors, 2018: JRA-55 based surface dataset for driving ocean-sea-ice models (JRA55-do). *OCEAN MODELLING*, **130,** 79-139.